Acta Pharmaceutica Sinica B 2026;16(4):2474−2497

Chinese Pharmaceutical Association
Institute of Materia Medica, Chinese Academy of Medical Sciences

Acta Pharmaceutica Sinica B

www.elsevier.com/locate/apsb
www.sciencedirect.com

ORIGINAL ARTICLE

An oral immune enhancer with excellent biocompatibility for effectively strengthening body's immunity and treating cancer

Anqi Xie[a,b,†], Lei Feng[a,†], Yaping Shao[d,†], Yiqun Wan[a,c], Ying Zhang[a], Zheyi Liu[e], Haihua Ji[a], Hao Wan[a,*]

[a]*State Key Laboratory of Food Science and Resources, Nanchang University, Nanchang 330047, China*
[b]*College of Food Science and Technology, Nanjing Agricultural University, Nanjing 210095, China*
[c]*School of Chemistry and Chemical Engineering, Nanchang University, Nanchang 330031, China*
[d]*Liaoning Provincial Key Laboratory for Research on the Pathogenic Mechanisms of Neurological Diseases, The First Affiliated Hospital, Dalian Medical University, Dalian 116021, China*
[e]*CAS Key Laboratory of Separation Sciences for Analytical Chemistry, Dalian Institute of Chemical Physics, Chinese Academy of Sciences, Dalian 116023, China*

Received 28 July 2025; received in revised form 26 October 2025; accepted 8 December 2025

KEY WORDS

Immuno-enhancing effect;
Anoectochilus formosanus polysaccharides;
Structural characterization;
Biocompatibility;
Lactobacillus plantarum;
Single-cell coating;
Gut microbiota modulation;
Tumor immune microenvironment

Abstract Enhancing immunity offers a versatile yet effective strategy for treating or preventing diseases. Here, we obtained a new polysaccharide (AFP-80) from *Anoectochilus formosanus* that unexpectedly stimulated immune systems without causing any detectable adverse effects. AFP-80 was applied to encapsulate *Lactobacillus plantarum* (LP), a probiotic with immunoregulatory properties, through bridging by Fe^{3+}−tannic acid network (Fe−TA) to establish an oral immune enhancer (LP@Fe-TA@AFP-80). Upon oral administration, LP@Fe-TA@AFP-80 colonized intestines with high survival rates, aided by gastrointestinal stress-shielding and adhesive properties of AFP-80 and Fe−TA, respectively, leading to synergistic immuno-enhancing effects through combining AFP-80 and live LP. As a result, in immunocompromised mice, LP@Fe-TA@AFP-80 significantly renovated immune functions, which was deciphered to be closely associated with the rebalance of gut microbiota toward a profile with positively-immunoregulatory bacteria enriched as well as the involvement of peroxisome proliferators-activated receptor signaling pathway activation. Additionally, LP@Fe-TA@AFP-80 effectively treated cancer, *e.g.*, 4T1 breast and MC38 colon tumors, either alone or in combination with immune checkpoint blockade therapy, by remodeling tumor immune microenvironment and gut microbiota. Moreover,

*Corresponding author.
E-mail address: wanhao424@ncu.edu.cn (Hao Wan).
†These authors made equal contributions to this work.
Peer review under the responsibility of Chinese Pharmaceutical Association and Institute of Materia Medica, Chinese Academy of Medical Sciences.

https://doi.org/10.1016/j.apsb.2026.01.041
2211-3835 © 2026 The Authors. Published by Elsevier B.V. on behalf of Chinese Pharmaceutical Association and Institute of Materia Medica, Chinese Academy of Medical Sciences. This is an open access article under the CC BY-NC-ND license (http://creativecommons.org/licenses/by-nc-nd/4.0/).

LP@Fe-TA@AFP-80 demonstrated excellent biocompatibility, as directly revealed by negligible biotoxicity even after 6 months of consecutive ingestion, highlighting its great potential to be implemented into people's daily life for disease prevention.

© 2026 The Authors. Published by Elsevier B.V. on behalf of Chinese Pharmaceutical Association and Institute of Materia Medica, Chinese Academy of Medical Sciences. This is an open access article under the CC BY-NC-ND license (http://creativecommons.org/licenses/by-nc-nd/4.0/).

1. Introduction

The intricate interplay between immune homeostasis and disease suppression has long been recognized, prompting decades of efforts to develop immune enhancers to prevent and confront various diseases[1,2]. Immune enhancers are substances that stimulate or augment the activity of the immune system, thereby strengthening the body's capacity to combat infections, cancer, and other diseases[3,4]. Based on their origin, they are generally classified into two categories: synthetic and natural immune enhancers[5]. Synthetic immune enhancers include compounds such as cytokine analogs, Toll-like receptor (TLR) agonists, CpG oligonucleotides, and various polymeric or nanoparticle-based adjuvants[6]. These agents are widely employed in modern clinical practice, particularly as adjuvants in vaccines, where they boost antigen-specific immunity, and in cancer immunotherapy, where they amplify antitumor responses or improve checkpoint blockade efficacy[7]. Despite their potency, synthetic enhancers often face significant limitations, including but not limited to toxic tissue accumulation[8], provocation of undesired inflammatory reactions[9], and induction of long-term immune dysfunction[10]. Furthermore, synthetic immune enhancers are generally administered *via* injection and require medical supervision, which may limit their applicability for routine or long-term use[11]. In comparison, natural immune enhancers derived from food, plants, fungi, or animals are generally considered safer and have attracted increasing attention as promising strategies to boost immune function in diverse populations[12]. They have been already applied in diverse preclinical or clinical contexts, such as β-glucan used as an adjuvant in cancer therapy and immunonutrition, lentinan (from *Lentinula edodes*) as a supportive anticancer immunomodulator[13], saponins (*e.g.*, QS-21) in licensed vaccines[14], and garlic-derived nanoparticles (GNPs) with excellent biocompatibility reported to reinforce the immune checkpoint blockade therapy[15]. Their superior biocompatibility and suitability for oral administration align well with patient preferences and daily lifestyle integration, making them attractive not only for therapeutic interventions but also for incorporation into routine health maintenance[16]. Despite these advantages in safety and compliance, natural enhancers are often limited by heterogeneous composition, variability in efficacy, and relatively weaker potency compared to synthetic agents[17,18], highlighting the need for further research and innovation to optimize their efficacy through structural modification, synergistic formulations, or combination therapies, thereby expanding their clinical utility.

Probiotics are a major category of food supplements with low cost and easy accessibility[19]. The immunomodulatory effects of some orally administrated probiotics and their underlying mechanisms have progressively been elucidated, such as pathogen-associated molecular patterns (PAMPs)-induced immune responses and modulation of gut microbiota[20]. To date, various studies have already documented the immunomodulatory effects of probiotics, particularly *Lactobacillus plantarum* (LP), on strengthening body's immunity[21]. However, probiotics alone are difficult to confer sufficient therapeutic or preventive effects against diseases through regulating immunity due to their high sensitivity to gastrointestinal stresses (*e.g.*, gastric acids and bile salts)[22]. As such, encapsulation methods, such as single-cell coating and microcapsule encapsulation by synthetic polymers[23,24], applied to protect probiotics have sparked considerable attentions, of which the selection of appropriate encapsulation wall matrix with sufficient protection efficacy is crucial to preserving the bioactivity of probiotics orally administrated[25].

Polysaccharides, a major category of ingredients in various kinds of foods (*e.g.*, vegetables and fruits), can be selectively metabolized by gut microbiota to confer beneficial effects to the host[26]. Several studies have preliminarily revealed the ability of polysaccharides to enhance both cellular and humoral immunity after oral administration, which rendered them ideal candidates for the development of oral immune enhancers[27]. Moreover, given the intrinsic polymer structure, polysaccharides demonstrate to be an ideal category of encapsulation wall matrixes in probiotic oral delivery, revealing the potential to not only improve the bioavailability of probiotics but also to exploit the synergistic effect between polysaccharides and probiotics for better applications. *Anoectochilus formosanus* has been regarded as "food as medicine" in China dating back to the Ming dynasty due to its edible properties and broad applications in treating inflammation, detoxification, and alleviating throat infections[28]. The methanol extract from *A. formosanus* has been reported to inhibit the proliferation of the SCC-25 oral cancer cells by decreasing both mRNA and protein levels of programmed death 1-ligand 1 (PD-L1), an important regulator of activated T cells and tumor interaction, suggesting the potential application of *A. formosanus* in the immune checkpoint blockade therapy of cancer[29]. Notably, *A. formosanus* polysaccharides (AFP) are recognized as a category of macromolecules in *A. formosanus* with high bioactivities, exhibiting various functions like immune stimulation and anti-tumor effects[30]. For instance, it was inferred that AFP could enhance the immune activity of splenic lymphocytes *in vitro* by facilitating lymphocyte proliferation, increasing nitric oxide (NO) production, and promoting the secretion of cytokines (*e.g.*, interleukin-2, IL-2; interleukin-6, IL-6; and interferon-γ, IFN-γ)[31]. Moreover, there are also some reports suggesting the potential of AFP as prebiotics, which may contribute to maintaining intestinal immunity and promoting overall human intestinal health through immune regulation[32]. Previously, our group preliminarily discovered that oral consumption of crude polysaccharide mixtures extracted from *A. formosanus* (AFP) demonstrated certain immunomodulatory effects both *in vitro* and *in vivo*[33]. Theoretically, some refined polysaccharides within the crude AFP are anticipated to be able to strengthen body's immunity. This inspired us to leverage refined polysaccharides dug from the crude AFP for equipping probiotics with the immunoregulatory attribute, which capitalizes on the

inherent bioactivities, biocompatibility, and biodegradability of these polysaccharides to establish a bio-safe platform for probiotic oral delivery, aiming to secure an effective oral immune enhancer by taking advantage of synergistic immunoregulatory effects.

Herein, we discovered and obtained a natural refined polysaccharide (AFP-80) from *A. formosanus*, which unexpectedly demonstrated immunostimulatory properties without causing any detectable adverse effects. AFP-80 was applied to arm LP at the single-cell level by simple agitation through a bridging strategy based on Fe^{3+}−tannic acid (two substances existing in various kinds of food[34,35]) network (Fe−TA) recently developed by our group to construct an oral immune enhancer (LP@Fe-TA@AFP-80) for efficiently strengthening the host's immunity[36]. The approach for formulating the oral immune enhancer was featured by its simplicity and rapidity (the whole process took only ∼15 min by just agitating), beneficial for industrial translation. Moreover, as components constructing LP@Fe-TA@AFP-80 were derived from food-based sources, the immune enhancer revealed excellent biocompatibility as directly confirmed by observing negligible biotoxicity even after consecutive oral administration on 2 days' basis (1×10^8 CFU/mL every time) for 6 months. Upon ingestion of LP@Fe-TA@AFP-80, AFP-80 acted as a stable and firm barrier to refrain gastrointestinal stresses from attacking LP, after which live LP colonized within intestines aided by Fe-TA due to its adhesive ability toward the intestinal mucous layer by forming hydrogen bonds, thus working with AFP-80 to exert a synergistic effect for strengthening the immunity. As a result, LP@Fe-TA@AFP-80 succeeded in augmenting humoral/intestinal immunity, restoring the intestinal barrier, promoting the secretion of immunostimulatory cytokines, and enhancing the body's antioxidative ability in immunocompromised mice, of which the underlying mechanism was deciphered to be strongly related to the restoration of the dysbiosis of gut microbiota and the involvement of activation of peroxisome proliferators-activated receptor (PPAR) signaling pathway. Notably, taking advantage of the satisfactory immunoenhancing effect, LP@Fe-TA@AFP-80 also achieved to inhibit tumor growth as well as to eradicate tumors in combination with the blockade of immune checkpoint PD-L1, highlighting its potential as an effective oncology therapeutic. Given the critical role of immune functions in the development and progression of various diseases, this oral immune enhancer shows promise for preventing and treating a wide range of diseases and could be implemented into daily health regimens due to its excellent biocompatibility.

2. Materials and methods

2.1. Materials

A. formosanus was obtained from Taiwan province, China. The monosaccharide standards, such as D-Galactose and L-Arabinose, were obtained from Merck Co., Ltd. (Darmstadt, Germany). Levamisole hydrochloride (LH) along with cyclophosphamide (Cy) were acquired from Shanghai Aladdin Biochemical Technology Co., Ltd. (Shanghai, China). Cytokine (immunoglobulin A, IgA; immunoglobulin G, IgG; IL-6; interleukin-10, IL-10; IFN-γ; and tumor necrosis factor-α, TNF-α) detecting ELISA kits were obtained from Fcmacs Biotech Co., Ltd. (Nanjing, China). NO detecting ELISA kit was provided by Nanjing Jiancheng Technology Co., Ltd. (Nanjing, China). Lipopolysaccharide (LPS) and phosphate buffer saline (PBS) buffer powder were purchased from Beijing Solarbio Science & Technology Co., Ltd. (Beijing, China). Tannic acid (TA) was purchased from Sigma−Aldrich (St. Louis, MO, USA). De Man, Rogosa and Sharpe (MRS) culture medium was purchased from Qingdao Hi-tech Industrial Park Hope Bio-technology Co., Ltd. (Qingdao, China). The assay kits for total antioxidant capacity (T-AOC), superoxide dismutase (SOD), malondialdehyde (MDA), glutathione peroxidase (GSH-px), Dulbecco's modified Eagle's medium (DMEM), Roswell Park Memorial Institute (RPMI) 1640 medium, and fetal bovine serum (FBS) were purchased from Wuhan Servicebio Technology Co., Ltd. (Wuhan, China). The reagents employed in this study were of analytical grade.

2.2. Strain culture

LP was obtained from the Beijing Baioubowei Biotechnology Co., Ltd. (Beijing, China). The probiotics were cultured in liquid MRS medium in a shaker (37 °C, 200 rpm/min).

2.3. Cell culture

RAW264.7 cells, 4T1 mouse breast cancer cells, and MC38 mouse colon cancer cells were sourced from Procell Life Science & Technology Co., Ltd. (Wuhan, China). RAW264.7 cells were grown in DMEM enriched with 10% FBS and 1% penicillin−streptomycin. Meanwhile, both 4T1 mouse breast cancer cells and MC38 mouse colon cancer cells were cultured in RPMI 1640 medium that was enriched with 10% FBS and 1% penicillin−streptomycin. All types of cells were cultivated under a controlled environment of 37 °C with a moisture-saturated atmosphere that contained 5% carbon dioxide (CO_2).

2.4. Purification of AFP

AFP was extracted and purified following our previous protocol with minor modifications[37]. The fractions of AFP with various molecular weights were separated by graded ethanol precipitation, taking advantage of the solubility differences of polysaccharides with different molecular weights in ethanol. In short, 300 mg of AFP were dissolved in 30 mL of distilled water and precipitated with ethanol at a concentration of 20%, 60%, and 80%, respectively. The precipitates were washed 3 times with anhydrous ethanol and acetone. After redissolving, dialyzing, concentrating, and lyophilizing, three fractions purified from AFP were labeled as AFP-20, AFP-60, and AFP-80-C, respectively.

Subsequently, AFP-80-C was loaded onto a DEAE Sepharose Fast Flow column (6 cm × 58 cm) and was eluted sequentially with water and NaCl solutions at concentrations of 0.2, 0.3, or 0.4 mol/L with a flow rate of 1.0 mL/min. The obtained polysaccharide samples were designated as AFP-80-C-water, AFP-80-C-0.2, AFP-80-C-0.3, and AFP-80-C-0.4, respectively. The main fraction (AFP-80-C-0.4) with the highest yield was collected, dialyzed, and then lyophilized to produce the homogenous polysaccharide referred to as AFP-80.

The homogeneity and molecular weight of polysaccharide fractions were assessed using HPGPC[38]. The monosaccharides were determined according to a previous study[39]. Acidic polysaccharides were reduced using $NaBD_4$, and the glycosidic linkages of three refined AFP fractions were analyzed. The ^{13}C NMR, ^1H NMR, $^1H/^1H$ correlation spectroscopy (COSY), total correlation spectroscopy (TOCSY), heteronuclear single quantum

coherence (HSQC), heteronuclear multiple bond correlation (HMBC), and nuclear overhauser effect spectroscopy (NOESY) spectra of the three refined AFP fractions were measured on a Bruker AVANCE HD III 600 MHz Spectrometer (Bruker, Rheinstetten, Germany) at 293 K. The ^{1}H NMR spectrum was recorded by fixing HOD signal at δ 4.70 ppm.

2.5. Evaluation of immuno-enhancing effect of refined AFP in vitro

To evaluate the immuno-enhancing activity of refined AFP, RAW264.7 cells were plated in 6-well plates with a density of 10^5 cells/well and cultured for 24 h, and then incubated with different concentrations of AFP-20, AFP-60, AFP-80 (0, 50, 100, 200, and 400 μg/mL) or LPS for additional 24 h. Each well received 100 μL diluted CCK-8 solution and was incubated for 24 h. The absorbance was quantified using a microplate reader (Thermo Fisher Scientific, Shanghai, China) at 450 nm. A Griess reagent kit was used to measure NO production. The absorbance was monitored with the microplate reader at 540 nm. After measuring NO levels, the culture supernatants from the macrophage cells were collected to quantify the production of TNF-α and IL-6, utilizing the corresponding ELISA kits.

2.6. Synthesis and characterization of LP@Fe-TA@AFP-80

LP were incubated overnight at 37 °C in 5 mL of MRS medium with shaking at 200 rpm. The bacteria were then obtained by centrifugation at 6000 rpm for 4 min, washed twice with PBS, and resuspended in 1 mL of PBS. The detailed preparation process of LP@Fe-TA was described in our previous research[36] The sediment of LP@Fe-TA was subsequently mixed with 990 μL PBS buffer (pH 5.0). using a gentle vortex method. Then different concentrations of AFP-80 solutions were added to achieve a final concentration ranging from 0 to 1.6 mg/mL. After two additional washes with PBS, the LP@Fe-TA@AFP-80 complex was obtained. The Zetasizer (Pro, Malvern, UK) was utilized to measure the average sizes and zeta potentials of LP@Fe-TA@AFP-80. The morphology was observed by scanning electron microscopy (SEM) (Hitachi S-4800, Tokyo, Japan) and transmission electron microscopy (TEM) (HT7800, Tokyo, Japan). The method for the fluorescent labeling of AFP-80 was carried out according to the previous study with a few modifications[36]. DMSO was used to dissolve AFP-80, fluorescein isothiocyanate (FITC), dibutyltin dilaurate, and pyridine, which were then stirred overnight in a dark environment. After this process, dialysis and lyophilization were performed to yield purified FITC-labeled AFP-80. The FITC-labeled LP@Fe-TA@AFP-80 was synthesized using the same aforementioned method, with FITC-labeled AFP-80 incorporated into the structure. Subsequently, laser scanning microscopy (LEICA TCS SP8, Wetzlar, Germany) was employed for confocal laser scanning microscope (CLSM) analysis of the samples.

2.7. Growth curves of LP@Fe-TA@AFP-80

The LP, LP@Fe-TA, and LP@Fe-TA@AFP-80 samples were introduced into fresh MRS medium, achieving an OD_{600} of 0.15. Subsequently, the samples were cultured in a controlled environment at 37 °C with mild agitation and were measured every 2 h over a duration of 24 h using a microplate reader.

2.8. In vitro resistance of LP@Fe-TA@AFP-80 to gastrointestinal conditions

Equivalent amounts of LP, LP@Fe-TA, and LP@Fe-TA@AFP-80 (1×10^8 CFU/mL) were introduced into 1.6 mL simulated gastric fluid (SGF, pH 2.5, consisting of 1000 mL distilled H_2O, 5 g pepsin, 8.5 g NaCl) for 2 h and 4% bile salts for 3 h, respectively, for testing. Additionally, equivalent amounts of LP, LP@Fe-TA, and LP@Fe-TA@AFP-80 were also placed under conditions mimicking the gastrointestinal conditions (initially incubated in SGF for 2 h before being transferred to simulated intestinal fluid [SIF] comprising phosphate buffer at pH 7.4 with 1.60 mg/mL of trypsin added for 1 h). Subsequently, the solution was stirred at 200 rpm and incubated at 37 °C. An aliquot of 300 μL from the reaction mixture was taken at designated time intervals, centrifuged to precipitate the components, and washed with PBS. The resulting suspension was applied to solid MRS plates following a series of dilutions. Following incubation at 37 °C for 24 h, the colonies were counted.

2.9. Animals

The female BALB/c mice aged 6−8 weeks and weighing about 20 ± 0.2 g were obtained from GemPharmatech Co., Ltd. (Nanjing, China) and raised in an SPF-rated environment under a 12 h light/dark cycle with sterilized food pellets and distilled water. The temperature for the housing room was about 24 °C and the humidity was about 50%. All animal studies were carried out following the guidelines approved by the Institutional Animal Care and Use Committee of Nanchang University [No. SYXK (Gan) 2021-0004].

2.10. Biocompatible evaluation

For the acute oral biotoxicity study, the OECD Test Guidelines 425 with some modifications was employed to test the acute oral toxicity of LP@Fe-TA@AFP-80 in mouse model[40]. A total of 12 female BALB/c mice (20 ± 0.2 g, 6−8 weeks) were used. After 7 days of acclimatization, mice were randomly divided into 2 groups ($n = 6$) and were administered with 200 μL saline (normal group) or LP@Fe-TA@AFP-80 suspension (1×10^{12} CFU/mL, high-dose group), where the dose was determined by previous research[41], at the first day once according to their assignments. The physiological conditions of the mice were then observed, including body weight, abnormal behaviors (if any), and death (if any), and the mice were sacrificed after 14 days for further biocompatible analysis.

A sub-acute oral biotoxicity study lasting 28 days was conducted in accordance with the OECD Test Guideline 407 with minor modifications[42]. A total of 18 female BALB/c mice (20 ± 0.2 g, 6−8 weeks) were used. After seven days of acclimatization, the mice were randomly assigned to three groups ($n = 6$): normal group, medium-dose group, and low-dose group. Each group received daily administration of 200 μL saline (normal group) or LP@Fe-TA@AFP-80 suspension at different concentrations (1×10^{10} CFU/mL, denoted as medium-dose group; 1×10^9 CFU/mL, denoted as low-dose group). The physiological conditions of the mice were then observed, including body weight, abnormal behaviors (if any), and death (if any), and the mice were sacrificed after 28 days for further biocompatible analysis.

The long-term biosafety of LP@Fe-TA@AFP-80 was assessed through a 6-month toxicity study. A total of 12 female BALB/c

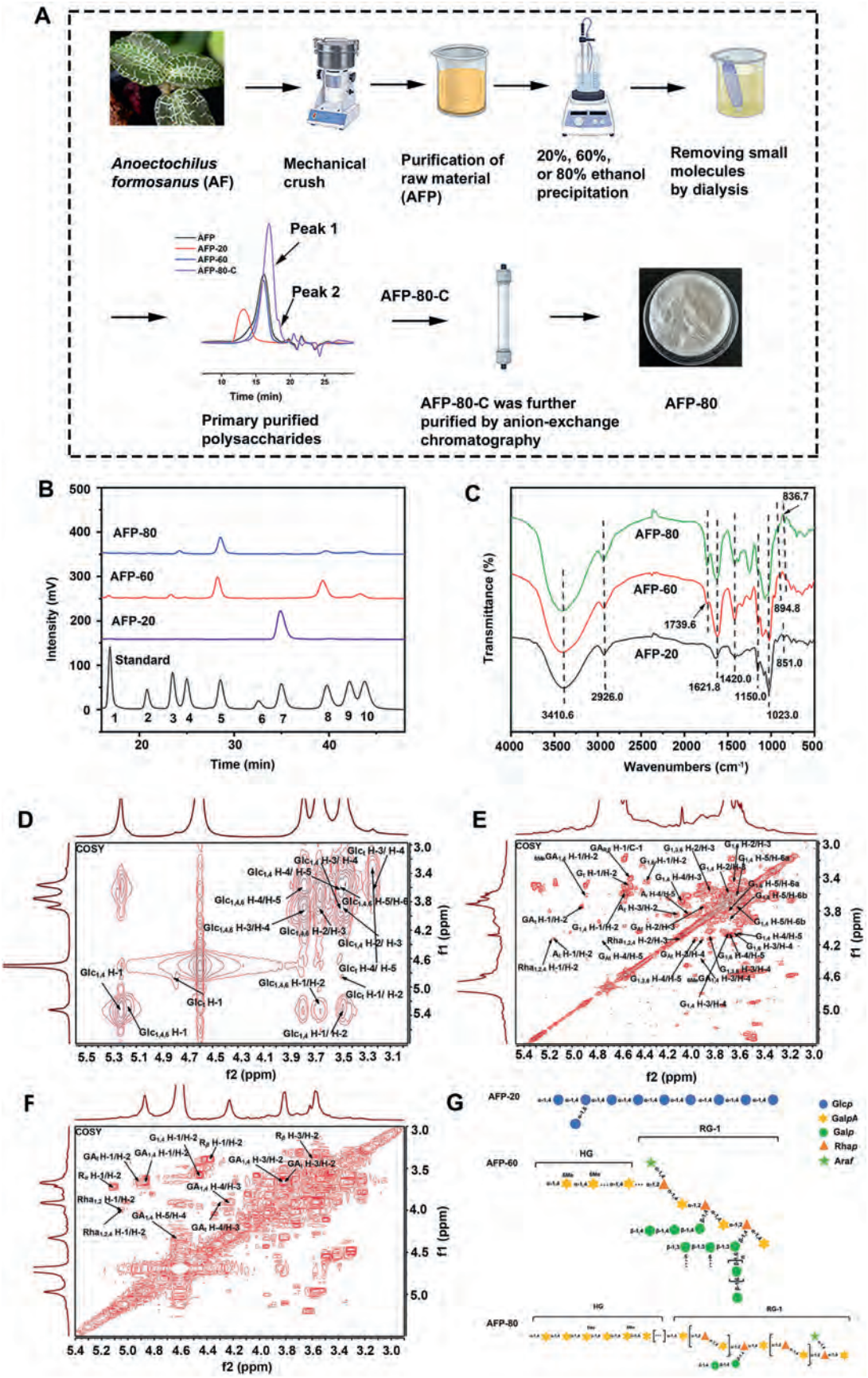
A
Anoectochilus formosanus (AF)
Mechanical crush
Purification of raw material (AFP)
20%, 60%, or 80% ethanol precipitation
Removing small molecules by dialysis
AFP
AFP-20
AFP-60
AFP-80-C
Peak 1
Peak 2
Time (min)
Primary purified polysaccharides
AFP-80-C
AFP-80-C was further purified by anion-exchange chromatography
AFP-80
B
AFP-80
AFP-60
AFP-20
Standard
Intensity (mV)
Time (min)
C
AFP-80
AFP-60
AFP-20
836.7
894.8
851.0
1739.6
1621.8
1420.0
1150.0
2926.0
3410.6
1023.0
Transmittance (%)
Wavenumbers (cm⁻¹)
D
COSY
f2 (ppm)
f1 (ppm)
E
COSY
f2 (ppm)
f1 (ppm)
F
COSY
f2 (ppm)
f1 (ppm)
G
AFP-20
AFP-60
AFP-80
HG
RG-1
Glcp
GalpA
Galp
Rhap
Araf

mice (20 ± 0.2 g, 6−8 weeks) were randomly assigned to two groups ($n = 6$): the normal group and LP@Fe-TA@AFP-80 group after seven days of acclimatization. Mice were administered with 200 μL LP@Fe-TA@AFP-80 (1×10^8 CFU/mL) or saline *via* gavage every other day for consecutive 180 days according to their group assignment. The animals were monitored every two days for any alterations in their behaviors. The mice were euthanized for additional biocompatible analysis after 6 months.

At the end of each experiment, the blood of mice from each group was collected and the serum biochemistry analysis was performed, including alanine aminotransferase (ALT), aspartate transaminase (AST), total bilirubin (T-BIL), lactate dehydrogenase (LDH), CR, urea, and uric acid (UA). Main organs (*i.e.*, liver, spleen, kidney, and thymus) were weighed, sectioned, and stained with hematoxylin−eosin (H&E). The organ indices were determined according to Eq. (1):

$$\text{Organ index}\ (\%) = \frac{\text{Organ weight}\ (\text{g})}{\text{Body weight}\ (\text{g})} \times 100 \quad (1)$$

2.11. Evaluation of the treatment effect of LP@Fe-TA@AFP-80 toward immunocompromised mice

After a one-week adaptive feeding, an immunocompromised model was constructed by Cy treatment of BALB/c mice weighing about 20 g. Briefly, all the mice were randomly assigned to seven groups: normal group, model group, AFP-80 (40 mg/kg BW) group, LP (1×10^8 CFU/mL) group, AFP-80 (40 mg/kg BW) + LP (1×10^8 CFU/mL) group, LP@Fe-TA@AFP-80 (1×10^8 CFU/mL) group, and positive group (LH, 40 mg/kg BW). Except for the normal group, the remaining groups were all intraperitoneally injected with 80 mg/kg BW of Cy for three consecutive days to induce immunocompromise in mice. In contrast, the normal group was intraperitoneally injected with saline. The body weight served as a measure to confirm the successful establishment of the immunocompromised mouse model. During 7 days of treatment, the mice in the normal and model groups were orally administrated with saline once daily, while the remaining five groups were orally administrated with the corresponding formulations based on their group assignment. After 7 days of therapy, the mice were sacrificed and the major organs were collected for further analysis.

2.12. ELISA assay

The levels of IgA and IgG in the serum, IL-6 and TNF-α in the spleen, IL-8 and IL-1β in the intestine, as well as MDA, GSH-px, SOD, and T-AOC in the liver were quantified using corresponding ELISA assay kits according to the guidelines provided by the manufacturer.

2.13. Immunofluorescence staining analysis

Immunofluorescence staining was conducted to assess the expression levels of ZO-1 and Occludin, as well as to characterize $CD4^+$ T cells and $CD8^+$ T cells in the collected tissues. After incubating tissue sections with primary antibodies (anti-ZO-1, anti-Occludin, anti-$CD4^+$, and anti-$CD8^+$) and fluorophore-labeled secondary antibodies, alterations in the levels of ZO-1, Occludin, $CD4^+$, and $CD8^+$ T cells were examined using a fluorescence microscope. The mean fluorescence density was assessed using Image-J analysis software[43].

2.14. Western blotting

The intestinal tissues were washed with pre-cooled PBS 2 times and homogenized with 10 times RIPA buffer under the presence of a protease inhibitor. The protein samples were prepared and separated on 10% SDS-PAGE gel electrophoresis and transferred to polyvinylidene difluoride (PVDF) membranes. Then, the membrane was blocked with 5 mL of 5% non-fat dry milk in the shaker for 30 min. After washing, the samples were probed overnight at 4 °C with antibodies specific for PPARγ and βactin. Moreover, the membranes were rinsed and then incubated for 30 min at room temperature with a peroxidase-conjugated secondary antibody.

2.15. Tumor therapy experiments

1×10^6 4T1 mouse breast cancer cells were subcutaneously injected into each BALB/c mouse to establish the 4T1 tumor-bearing mice. When the tumor reached about 100 mm^3, the 4T1 tumor-bearing mice were randomly divided into five groups ($n = 5$ per group): saline, LP, AFP-80, AFP-80 + LP, and LP@Fe-TA@AFP-80. Mice were orally treated with various formulations daily (LP, 1×10^8 CFU/mL; AFP-80, 40 mg/kg BW; AFP + LP, 40 mg/kg BW for AFP and 1×10^8 CFU/mL for LP; LP@Fe-TA@AFP-80, 1×10^8 CFU/mL) for 14 days. The body weights and tumor volume were measured every two days. On the 15th day, the mice from each group were sacrificed and the contents of IL-10 and IFN-γ in serum were determined by ELISA kits. Their tumors were dissected and weighed. The tumor tissues were sectioned to perform H&E staining. To evaluate tumor cell proliferation, tumor paraffin sections were prepared to be stained with Ki67 according to the manufacturer's instructions. Cell nuclei were stained by DAPI. Furthermore, to profile CD206, iNOS, $CD4^+$, and $CD8^+$ in tumor tissues, sections of the tumors were incubated with primary antibody: anti-CD206 (1:200 dilution, Servicebio, China), anti-iNOS (1:2000 dilution, Servicebio, China), anti-CD4 (1:2000 dilution, Servicebio, China), and anti-CD8 (1:200 dilution, Servicebio, China), respectively, followed by 50 min incubation at room temperature with the appropriate

Figure 1 Extraction, purification, and characterization of refined polysaccharides. (A) Schematic of obtaining refined AFP and HPGPC profiles of AFP. AFP-20, AFP-60, and AFP-80-C were obtained by gradient alcohol precipitation. AFP-80-C was then purified by anion-exchange chromatography, leading to the isolation of a highly pure component, which was designated as AFP-80. (B) High-performance liquid chromatography (HPLC) chromatogram profiles of monosaccharide composition of AFP-20, AFP-60, and AFP-80. The monosaccharide standards are: 1. mannose, 2. glucosamine, 3. rhamnose, 4. glucuronic acid, 5. galacturonic acid, 6. galactosamine, 7. glucose, 8. galactose, 9. xylose, and 10. arabinose. (C) FT-IR spectra of AFP-20, AFP-60, and AFP-80. (D) The correlated spectroscopy (COSY) spectrum of AFP-20. (E) The COSY spectrum of AFP-60. (F) The COSY spectrum of AFP-80. (G) Predicted structures of the repeating units of AFP-20, AFP-60, and AFP-80.

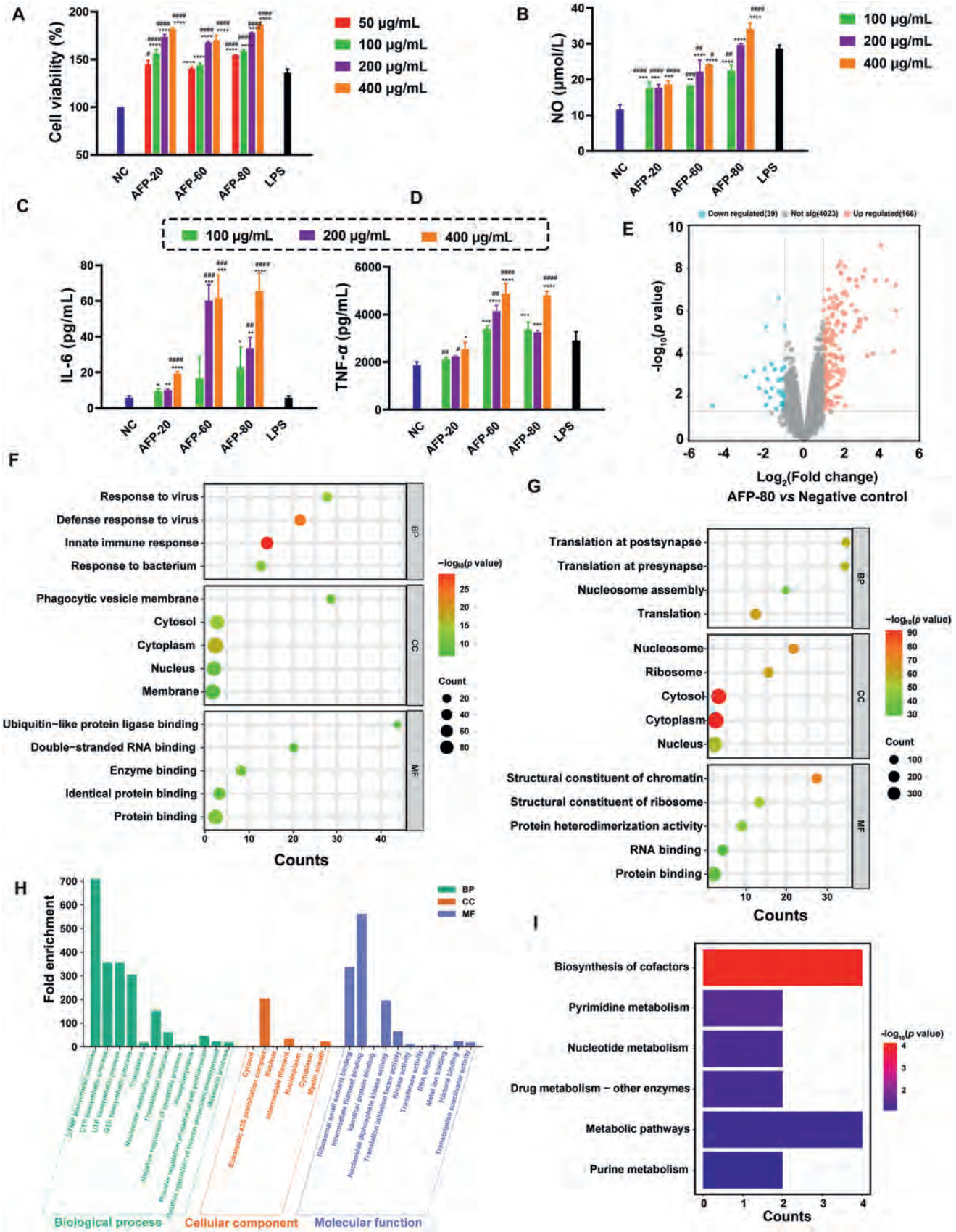
A
Cell viability (%)
50 μg/mL
100 μg/mL
200 μg/mL
400 μg/mL
NC
AFP-20
AFP-60
AFP-80
LPS
B
NO (μmol/L)
100 μg/mL
200 μg/mL
400 μg/mL
C
IL-6 (pg/mL)
D
TNF-α (pg/mL)
E
Down regulated(39)
Not sig(4023)
Up regulated(166)
-log10(p value)
Log2(Fold change)
AFP-80 vs Negative control
F
Response to virus
Defense response to virus
Innate immune response
Response to bacterium
Phagocytic vesicle membrane
Cytosol
Cytoplasm
Nucleus
Membrane
Ubiquitin-like protein ligase binding
Double-stranded RNA binding
Enzyme binding
Identical protein binding
Protein binding
BP
CC
MF
-log10(p value)
Count
Counts
G
Translation at postsynapse
Translation at presynapse
Nucleosome assembly
Translation
Nucleosome
Ribosome
Cytosol
Cytoplasm
Nucleus
Structural constituent of chromatin
Structural constituent of ribosome
Protein heterodimerization activity
RNA binding
Protein binding
Counts
H
Fold enrichment
BP
CC
MF
Biological process
Cellular component
Molecular function
I
Biosynthesis of cofactors
Pyrimidine metabolism
Nucleotide metabolism
Drug metabolism - other enzymes
Metabolic pathways
Purine metabolism
-log10(p value)
Counts

secondary antibodies. All the antibodies were used following the suppliers' protocols.

MC38 tumor-bearing mice were generated by subcutaneously injecting 5×10^5 MC38 cells into the left thigh. Once the tumor average volume reached between 80 and 100 mm^3, BALB/c mice were evenly divided into three groups. Mice receiving intraperitoneal injections of 200 μL of 10 mg/kg PD-L1 antibody 3 times per week were classified as the anti-PD-L1 group. Mice that were orally administered LP@Fe-TA@AFP-80 daily and concomitantly injected intraperitoneally with 10 mg/kg of PD-L1 antibody 3 times per week were denoted as the LP@Fe-TA@AFP-80 + anti-PD-L1 group. Control mice received the same volume of saline, designated as the saline group. Tumor volumes were assessed three times per week using caliper measurements and calculated according to Eq. (2):

$$\text{Tumor volume} = \text{Length} \times \text{Width}^2 \times 1/2 \quad (2)$$

The body weight was also recorded to assess toxicity.

2.16. 16S rRNA sequencing measurement

Feces samples from each group were collected from mice and stored at −80 °C for the following 16S rRNA sequencing analysis. In summary, microbial community DNA was extracted using the CTAB method, and sequencing libraries were prepared utilizing a TruSeq DNA PCR-Free Sample Preparation Kit (Illumina, USA) in accordance with the manufacturer's guidelines.

2.17. Statistical analysis

Data are presented as mean ± standard deviation (SD) and are processed using GraphPad Prism 8.0. Statistical comparisons were conducted using one-way analysis of variance (ANOVA) analysis or Student's *t* test. Significance levels were denoted as follows: $^*P < 0.05$, $^{**}P < 0.01$, $^{***}P < 0.001$, $^{****}P < 0.0001$.

3. Results and discussion

3.1. Characterization of refined polysaccharides obtained from *A. formosanus*

With the motivation to secure suitable refined polysaccharides for the construction of an oral immune enhancer, we first separated and characterized refined polysaccharides from *A. formosanus.* Crude AFP were obtained from *A. formosanus* by water extraction and alcohol precipitation, followed by precipitation of the crude AFP with ethanol at a concentration of 20%, 60%, and 80% (*v*/*v*), respectively, to acquire three polysaccharide fractions (namely AFP-20, AFP-60, and AFP-80-C) as illustrated in Fig. 1A (please see methods for detailed preparation processes). According to the HPGPC patterns depicted in Fig. 1A, a single peak was observed in AFP-20 and AFP-60, respectively, which indicated the high purity of these two fractions. For AFP-80-C, two peaks (*i.e.*, peaks 1 and 2) were found in its HPGPC profile. Considering the dark color of AFP-80-C, we hypothesized that pigmentary impurities might result in the observed double peaks. In this case, further purification of AFP-80-C was performed through anion-exchange chromatography and eluted sequentially with NaCl aqueous solutions at concentrations of 0.0, 0.2, 0.3, or 0.4 mol/L (namely AFP-80-C-water, AFP-80-C-0.2, AFP-80-C-0.3, or AFP-80-C-0.4). Among eluted fractions, AFP-80-C-0.4 exhibited the highest yield of 48.50% and showed a much lighter color (Supporting Information Fig. S1). As shown in Supporting Informmation Fig. S2, only a single narrow peak (peak 1) was observed for AFP-80-C-0.4, indicating its high purity. Therefore, AFP-80-C-0.4 was selected and denoted as AFP-80 for further investigation. Based on the equation of the calibration curve of dextran and glucose (Supporting Information Fig. S3), the weight-average molecular weights (M_w) of AFP-20, AFP-60, and AFP-80 were determined to be 1.05×10^3, 17.37, and 14.73 kDa, respectively, suggesting their polymer structures.

To profile the compositions of these polysaccharides, major components constructing polysaccharides, including the neutral sugar and the uronic acid, were characterized for AFP-20, AFP-60, and AFP-80 according to the phenol-sulphuric acids method and meta-hydroxy diphenyl method, respectively[44]. The results were summarized in Supporting Information Table S1, revealing distinct profiles for AFP-20, AFP-60, and AFP-80. Specifically, AFP-20 was characterized by a higher proportion of neutral sugars, with comparatively lower levels of uronic acids compared with those of AFP-60 or AFP-80. Accordingly, the monosaccharide composition analysis indicated that AFP-20 was a glucan, while AFP-60 and AFP-80 could be classified as acidic polysaccharides (Fig. 1B), which was further evidenced by the Fourier Transform Infrared Spectroscopy (FT-IR) analysis as the absorption peaks at 1739.6 cm^{-1} corresponding to the uronic acid only appeared for AFP-60 and AFP-80 (Fig. 1C).

Furthermore, the structural information of AFP-20, AFP-60, and AFP-80 was obtained through their methylation followed by

Figure 2 Evaluation of the immunostimulatory attribute of refined AFP. (A) Cell viability of RAW264.7 after incubation with AFP-20, AFP-60, or AFP-80 for 24 h. LPS served as the positive control, and untreated cells were denoted as the negative control. (B) NO release from RAW264.7 was determined after incubation with AFP-20, AFP-60, or AFP-80 for 24 h. (C) Secretion of IL-6 from RAW264.7 cells after treatment with AFP-20, AFP-60, or AFP-80 for 24 h. (D) Secretion of TNF-α from RAW264.7 cells treated with AFP-20, AFP-60, or AFP-80 for 24 h. "NC" represented the negative control group. (E) Volcano plot for differentially expressed proteins of RAW264.7 cells after treatment with AFP-80 for 24 h *versus* untreated cells ($P < 0.05$, $|\log_2(\text{Fold Change})| > \log_2(2)$). (F) GO enrichment analysis of up-regulated proteins between the AFP-80 treatment group and the negative control group. The bubble diagram only displayed the top 5 GO function sets with the most significant enrichment in each classification. (G) GO enrichment analysis of down-regulated proteins between the AFP-60-treated macrophages and untreated macrophages. The bubble diagram only displayed the top 5 GO function sets with the most significant enrichment in each classification. (H) GO enrichment analysis of up-regulated proteins between the AFP-80-treated macrophages and LPS-treated macrophages. (I) KEGG enrichment analysis of up-regulated proteins between the AFP-80 treatment group and the LPS group. Data are presented as the mean ± SD ($n = 3$). Statistical comparisons were conducted using either one-way analysis of variance (ANOVA) or the Student's *t*-test. Significance levels were denoted as follows: $^*P < 0.05$, $^{**}P < 0.01$, $^{***}P < 0.001$, and $^{****}P < 0.0001$ were obtained through comparison with the negative control group. $^{\#}P < 0.05$, $^{\#\#}P < 0.01$, $^{\#\#\#}P < 0.001$, and $^{\#\#\#\#}P < 0.0001$ were obtained through comparison with the LPS group.

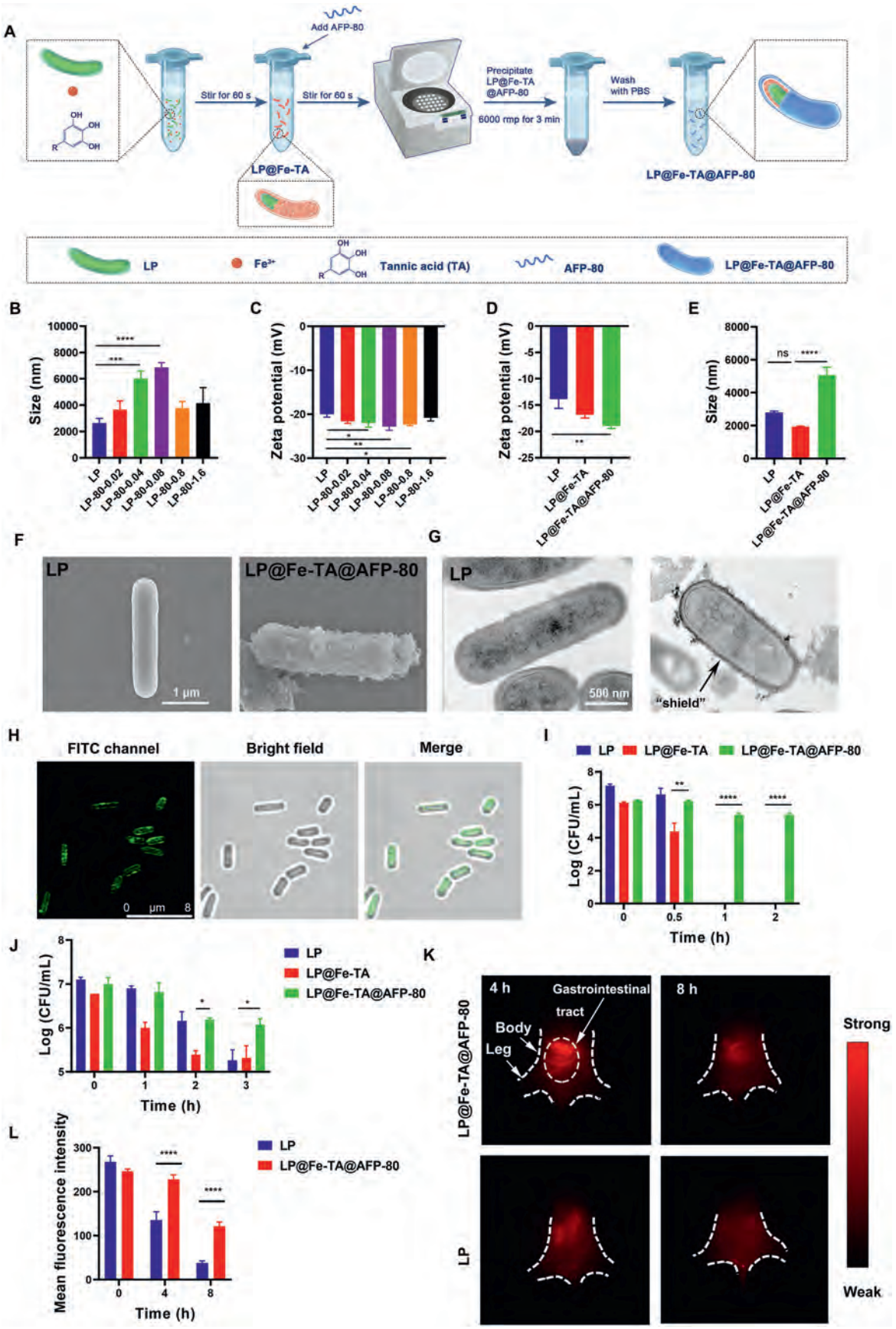
A
Add AFP-80
Stir for 60 s
Stir for 60 s
Precipitate LP@Fe-TA @AFP-80
6000 rmp for 3 min
Wash with PBS
LP@Fe-TA
LP@Fe-TA@AFP-80
LP
Fe3+
Tannic acid (TA)
AFP-80
LP@Fe-TA@AFP-80
B
Size (nm)
LP
LP-80-0.02
LP-80-0.04
LP-80-0.08
LP-80-0.8
LP-80-1.6
C
Zeta potential (mV)
D
Zeta potential (mV)
LP
LP@Fe-TA
LP@Fe-TA@AFP-80
E
Size (nm)
ns
F
LP
LP@Fe-TA@AFP-80
1 μm
G
LP
500 nm
"shield"
H
FITC channel
Bright field
Merge
0 μm 8
I
LP
LP@Fe-TA
LP@Fe-TA@AFP-80
Log (CFU/mL)
Time (h)
J
LP
LP@Fe-TA
LP@Fe-TA@AFP-80
Log (CFU/mL)
Time (h)
K
4 h
8 h
Gastrointestinal tract
Body
Leg
LP@Fe-TA@AFP-80
LP
Strong
Weak
L
LP
LP@Fe-TA@AFP-80
Mean fluorescence intensity
Time (h)

Gas Chromatography−Mass Spectrometry (GC−MS) analysis. As summarized in Supporting Information Table S2, AFP-20 was found to contain three main types of glucosyl residues assigned to α-D-Glc*p*-(1→, →4)-α-D-Glc*p*-(1→, and →4,6)-α-D-Glc*p*-(1→, respectively[37]. The corresponding molar ratio of the three linkages in AFP-20 was approximately 7.70:81.60:10.66, indicating that AFP-20 was mainly comprised of →4)-α-D-Glc*p*-(1→ in the backbone and was branched at *O*-6. The linkage patterns of AFP-60 and AFP-80 were summarized in Supporting Information Tables S3 and S4, respectively. According to the results, in addition to →4)-α-D-Gal*p*A-(1→ (38.03%) and →4)-β-D-Gal*p*-(1→ (21.25%), →2,4)-α-L-Rha*p*-(1→ (8.31%), →3,6)-β-D-Gal*p*-(1→ (6.49%), →6)-β-D-Gal*p*-(1→ (2.31%), α-D-Gal*p*A-(1→ (3.14%), β-D-Gal*p*-(1→ (6.08%), and α-L-Ara*f*-(1→ (7.15%) were also observed in AFP-60, suggesting that AFP-60 contained both patterns of homogalacturonan (HG) and rhamnogalacturonan-I (RG-I)[45]. The AFP-80 was deciphered to a branched hetero-polysaccharide, with →4)-α-D-Gal*p*A-(1→ (75.47%) as the backbone and →2,4)-α-L-Rha*p*-(1→ (1.77%) as the branching node. Besides, minor →4)-β-D-Gal*p*-(1→ (3.25%), →2)-α-L-Rha*p*-(1→ (4.31%), →4,6)-α-D-Gal*p*A-(1→ (0.94%), and →3,6)-β-D-Gal*p*-(1→ (0.75%) constructed the chain of polysaccharide, which was terminated by α-L-Ara*f*-(1→ (1.67%) and α-D-Gal*p*A-(1→ (8.59%) (Table S4). Based on the results of Nuclear Magnetic Resonance Spectroscopy (NMR) and methylation (see supporting notes for details of the NMR analysis process, Supporting Information Tables S5−S7, Fig. 1D−F, Supporting Information Figs. S4−S6), the predicted structures of the repeating units of AFP-20, AFP-60, and AFP-80 were displayed in Fig. 1G. According to previous research, all polysaccharides isolated from *A. formosanus* so far have been characterized as neutral polysaccharides[30,31,46,47]. Therefore, our study represented the first instance of obtaining acidic polysaccharides from *A. formosanus*.

3.2. AFP-80 stimulated immune responses without causing adverse effects

Enlightened by our previous findings that crude AFP demonstrated certain immunostimulatory effects[33], with refined AFP-20, AFP-60, and AFP-80 fully characterized in hand, we further investigated immunostimulatory activities of these refined polysaccharides, aiming to locate the candidate for subsequent construction of the oral immune enhancer. By co-culturing with RAW264.7 macrophages, a crucial kind of cells of the innate immune system[48], all AFP-20, AFP-60, and AFP-80 promoted macrophage proliferation in a concentration-dependent manner (Fig. 2A, $P < 0.0001$), achieving ∼33%, ∼25%, and ∼37% higher than that induced by lipopolysaccharides (LPS, a commonly used immunostimulatory agent with significant cytotoxicity emerging if high concentrations [≥10 μg/mL] are adopted[49], Supporting Information Fig. S7), respectively, when the concentration of 400 μg/mL was applied, which indirectly indicated the activation of macrophage. Activated macrophages would secrete inducible nitrous oxide synthase (iNOS), leading to the production of NO[50]. As shown in Fig. 2B, compared with untreated cells (*i.e.*, negative control), AFP-20-, AFP-60-, or AFP-80-induced NO production was significantly elevated in a dose-dependent manner, among which AFP-80 induced the highest production. In addition, the activation of macrophages always accompanied by the secretion of cytokines IL-6 and TNF-α, two important immunoregulatory cytokines[51]. As shown in Fig. 2C and D, the secretion of IL-6 and TNF-α showed a concentration-dependent manner for all macrophages treated with refined AFP, with acidic polysaccharides (*i.e.*, AFP-80 and AFP-60) demonstrating a stronger promotion of secretion than the neutral polysaccharide (*i.e.*, AFP-20). Collectively, these results indicated that refined AFP demonstrated the immunostimulatory activity, suggesting that the presence of the uronic acid along with a high degree of branching and low molecular weights for polysaccharides would contribute to an enhanced immunostimulatory effect, which provides a theoretical guidance to screen natural polysaccharides with potential immunostimulatory activities[52]. This bioactivity differs from that for polysaccharides isolated from *A. formosanus* reported in previous studies[30,31,46,47], which should be attributed to the structural and compositional differences between neutral and acidic polysaccharides[53].

To gain deeper insights, we investigated the immunostimulatory mechanisms of AFP-20, AFP-60, and AFP-80 by proteomics. The proteomics analysis demonstrated a notable up-regulation in the expression levels of only three proteins in the AFP-20 treatment group compared to the negative control (*i.e.*, untreated cells, Supporting Information Table S8), indicating negligible bioactivity. Comparatively, acidic polysaccharides exhibited a more potent macrophage-activating effect, as AFP-60 and AFP-80 significantly up-regulated 182 and 166 proteins, respectively, relative to the negative control (Supporting Information Fig. S8A, Fig. 2E, $P < 0.05$). Interestingly, we observed a large number of down-regulated proteins for the AFP-60 or LPS treatment group when compared to the negative control (*i.e.*, 494 and 162, respectively), while only 39 proteins were down-regulated for the

Figure 3 LP@Fe-TA@AFP-80 with improved tolerance to gastrointestinal stresses and enhanced intestinal colonization. (A) Schematic regarding the preparation of LP@Fe-TA@AFP-80. Briefly, LP suspension was agitated with TA and Fe^{3+} for 60 s to facilitate the self-assembly of a robust Fe−TA layer on LP (LP@Fe-TA). Subsequently, LP@Fe-TA was further stirred with AFP-80 for an additional 60 s to establish LP@Fe-TA@AFP-80. (B) Size distribution of LP@Fe-TA@AFP-80 coated with varying concentrations of AFP-80 (ranging from 0.02 to 1.6 mg/mL). (C) Zeta potential analysis of LP@Fe-TA@AFP-80 coated with varying concentrations of AFP-80 (ranging from 0.02 to 1.6 mg/mL). (D) Zeta potential analysis of LP, LP@Fe-TA, and LP@Fe-TA@AFP-80. (E) Size distribution of LP, LP@Fe-TA, and LP@Fe-TA@AFP-80. (F) SEM pictures of LP and LP@Fe-TA@AFP-80. Scale bar: 1 μm. (G) TEM pictures of LP and LP@Fe-TA@AFP-80. Scale bar: 500 nm. (H) CLSM images of LP@Fe-TA@AFP-80. Scale bar: 8 μm. FITC-labeled AFP-80 was visualized in the green channel. (I) The number of viable bacteria of LP, LP@Fe-TA, and LP@Fe-TA@AFP-80 after exposure to SGF (pH 2.5) for 2 h. (J) The number of viable bacteria of LP, LP@Fe-TA, and LP@Fe-TA@AFP-80 after exposure to 4% bile salts for 3 h. (K) *In vivo* fluorescence imaging of mice orally administrated with Cy5-labeled LP@Fe-TA@AFP-80 or Cy5-labeled LP at predetermined time points. (L) Mean fluorescence intensity of Cy5-labeled LP and Cy5-labeled LP@Fe-TA@AFP-80 remaining within the gastrointestinal tract in mice at different time points post administration. Data are presented as mean ± SD ($n = 3$). Statistical comparisons were conducted using either one-way analysis of variance (ANOVA) or the Student's *t*-test. Significance levels were denoted as follows: $^{*}P < 0.05$, $^{**}P < 0.01$, and $^{****}P < 0.0001$.

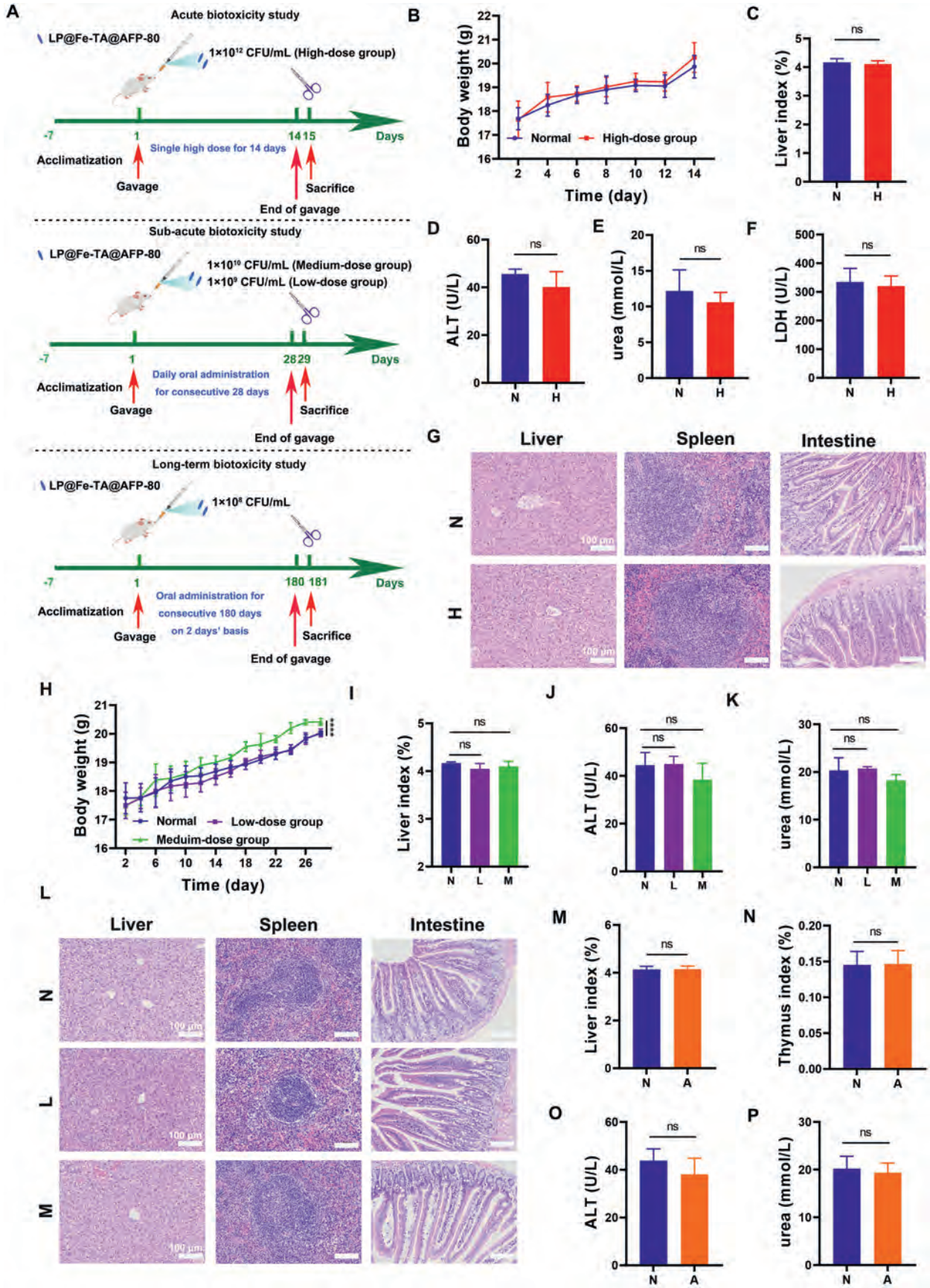
A
Acute biotoxicity study
LP@Fe-TA@AFP-80
1×10¹² CFU/mL (High-dose group)
-7
1
14 15
Days
Acclimatization
Gavage
Single high dose for 14 days
Sacrifice
End of gavage
Sub-acute biotoxicity study
LP@Fe-TA@AFP-80
1×10¹⁰ CFU/mL (Medium-dose group)
1×10⁹ CFU/mL (Low-dose group)
-7
1
28 29
Days
Acclimatization
Gavage
Daily oral administration for consecutive 28 days
Sacrifice
End of gavage
Long-term biotoxicity study
LP@Fe-TA@AFP-80
1×10⁸ CFU/mL
-7
1
180 181
Days
Acclimatization
Gavage
Oral administration for consecutive 180 days on 2 days' basis
Sacrifice
End of gavage
B
Body weight (g)
Normal
High-dose group
Time (day)
C
Liver index (%)
ns
N
H
D
ALT (U/L)
ns
E
urea (mmol/L)
ns
F
LDH (U/L)
ns
G
Liver
Spleen
Intestine
N
H
100 μm
H
Body weight (g)
Normal
Low-dose group
Meduim-dose group
Time (day)
I
Liver index (%)
ns
N
L
M
J
ALT (U/L)
ns
K
urea (mmol/L)
ns
L
Liver
Spleen
Intestine
N
L
M
100 μm
M
Liver index (%)
ns
N
A
N
Thymus index (%)
ns
O
ALT (U/L)
ns
P
urea (mmol/L)
ns

AFP-80 group, suggesting the more favorable biocompatibility of AFP-80 (Fig. S8 and Fig. 2E). Through Genes Ontology (GO) enrichment analysis, we identified significant enrichment of these two polysaccharides-up-regulated proteins in the domains associated with innate immunity and antiviral defense, suggesting that AFP-60 and AFP-80 exhibited similar immunostimulatory activity to the well-studied immunostimulant LPS (Supporting Information Figs. S9 and S10, Fig. 2F). Unexpectedly and interestingly, we observed a significant down-regulation of proteins associated with cytoplasmic translation after LPS or AFP-60 treatment (Supporting Information Fig. S11 and Fig. 2G), whereas AFP-80 did not exhibit such effects but instead up-regulated a greater number of proteins associated with the metabolism compared to LPS, demonstrating to be more biocompatible, as revealed by GO and Kyoto Encyclopedia of Genes and Genomes (KEGG) pathway enrichment analyses (Fig. 2H and I, Supporting Information Fig. S12). More specifically, KEGG enrichment analysis corroborated that AFP-60 or LPS suppressed macrophage biosynthesis by down-regulating both metabolic and ribosomal pathways (Supporting Information Fig. S13). To further elucidate the mechanism of macrophage activation by AFP-80 treatment, we performed KEGG pathway enrichment analysis on the up-regulated proteins relative to untreated macrophages (*i.e.*, negative control) and conducted Transcriptional Regulatory Relationships Unveiled by Sentence-based Text-mining (TRRUST) enrichment analysis. The results indicated that the NF-κB signaling pathway played a central role in AFP-80-mediated macrophage activation (Supporting Information Fig. S14). The immunostimulatory effects of AFP-80 were further confirmed on bone marrow-derived dendritic cells (BMDCs). According to the results, AFP-80 treatment significantly increased the proportion of $CD80^{+}CD86^{+}$ cells in BMDCs compared to untreated BMDCs (Supporting Information Fig. S15). In sum, these findings suggested that AFP-80 exerted the immunostimulatory capacity like LPS and AFP-60, but was much more biocompatible. Considering all above results, AFP-80 was selected for subsequent experiments.

3.3. Construction of LP@Fe-TA@AFP-80 with improved resistance to gastrointestinal stresses and sustained intestinal retention

After elucidating the structure and immunostimulatory effect of AFP-80, we were encouraged to apply AFP-80 as a "shield" to arm LP, a kind of probiotic which was reported to demonstrate certain immunoregulatory effects[33], aiming to not only improve their resistance but also achieve a synergistic immuno-enhancing effect for better strengthening the immunity *via* oral administration. Referring to our previous study[36], a continuous Fe−TA layer was firstly formed around LP to bridge AFP-80 (LP@Fe-TA@AFP-80) due to the formation of internal hydrogen bonds (see methods for the detailed fabrication process, Fig. 3A). To realize full encapsulation at the single-cell level for the best protection efficacy, the applied concentrations of AFP-80 were optimized. As depicted in Fig. 3B and C, the size and zeta potential of LP@Fe-TA@AFP-80 peaked when 0.08 mg/mL AFP-80 was applied, indicating the complete encapsulation of a single bacterium. This finding was further supported by the stepwise variation of zeta potential and size among LP, LP@Fe-TA, and LP@Fe-TA@AFP-80 (Fig. 3D and E). According to the growth curves and bacterial viability (Supporting Information Figs. S16 and S17), the encapsulation did not adversely affect the activity of LP. The SEM analysis, as depicted in Supporting Information Fig. S18 and Fig. 3F, clearly demonstrated the successful sequential encapsulation of LP with Fe-TA and AFP-80. This was evidenced by the morphological differences observed among LP, LP@Fe-TA, and LP@Fe-TA@AFP-80. Further corroboration was provided by TEM observation (Fig. 3G), which revealed a rougher surface and a thick coating for LP@Fe-TA@AFP-80 compared to naive LP. Additionally, CLSM imaging of LP@Fe-TA@AFP-80 revealed the position overlapping of the probiotics with FITC-labeled AFP-80 (see methods for the detailed labeling process), further identifying the successful construction of LP@Fe-TA@AFP-80 (Fig. 3H). Moreover, the robustness and universality of our encapsulation method were demonstrated by its successful application to *Escherichia coli* Nissle 1917 (EcN, a Gram-negative strain with negatively charged outer membrane) and *Clostridium weizmannii* (CW, a Gram-positive strain with a thick peptidoglycan cell wall and abundant surface-layer proteins)[54,55], in which effective single-cell encapsulation was consistently achieved (Supporting Information Fig. S19). These collective results established the presented method as a universal strategy for encapsulating a broad spectrum of probiotic bacteria toward various applications.

AFP-80 should behave like a "shield" due to its polymer structure to resist gastrointestinal assaults from attacking LP. To verify this, the viabilities of LP@Fe-TA@AFP-80 after experiencing gastrointestinal stresses, including SGF (pH 2.5), 4% bile salts, and conditions mimicking the entire gastrointestinal tract, were systematically evaluated. As revealed by Fig. 3I, neither LP nor LP@Fe-TA could survive after 1 h of incubation with SGF, while LP@Fe-TA@AFP-80 remained highly active even after 2 h

Figure 4 Evaluation of biocompatibility of LP@Fe-TA@AFP-80. (A) Experimental design for *in vivo* biocompatible evaluation of LP@Fe-TA@AFP-80. (B) Time−course body weight change of mice following treatment with saline (denoted as the normal group) or LP@Fe-TA@AFP-80 (1×10^{12} CFU/mL, denoted as the high-dose group) in the acute biotoxicity study. (C) Liver index of mice across various groups in the acute biotoxicity study. (D−F) Serum biochemistry analysis of mice across various groups in the acute biotoxicity study. (G) H&E staining of organs collected from mice after different treatments in the acute biotoxicity study. "N" was referred to as the normal group and "H" was referred to as the high-dose group. (H) Time−course body weight change of mice following treatment with saline or LP@Fe-TA@AFP-80 at different concentrations in the sub-acute biotoxicity study. (I) Liver index of mice across various groups in the sub-acute biotoxicity study. (J, K) Serum biochemistry analysis of mice across various groups in the sub-acute biotoxicity study. (L) H&E staining of organs collected from mice across various groups in the sub-acute biotoxicity study. "N" represented the normal group, "L" represented the low-dose group (1×10^{9} CFU/mL), and "M" represented the medium-dose group (1×10^{10} CFU/mL). (M) Liver index and (N) thymus index of mice across different groups in the long-term biotoxicity study. (O, P) Serum biochemistry analysis of mice across different groups in the long-term biotoxicity study. "N" represented the normal group and "A" represented the LP@Fe-TA@AFP-80 group (1×10^{8} CFU/mL). Data are presented as mean ± SD, with sample sizes of $n = 6$ for panels B, C, H, I, M and N; and $n = 3$ for panels D, E, F, J, K, O, and P. Statistical comparisons were conducted using either one-way analysis of variance (ANOVA) or the Student's *t*-test. ns means no significance.

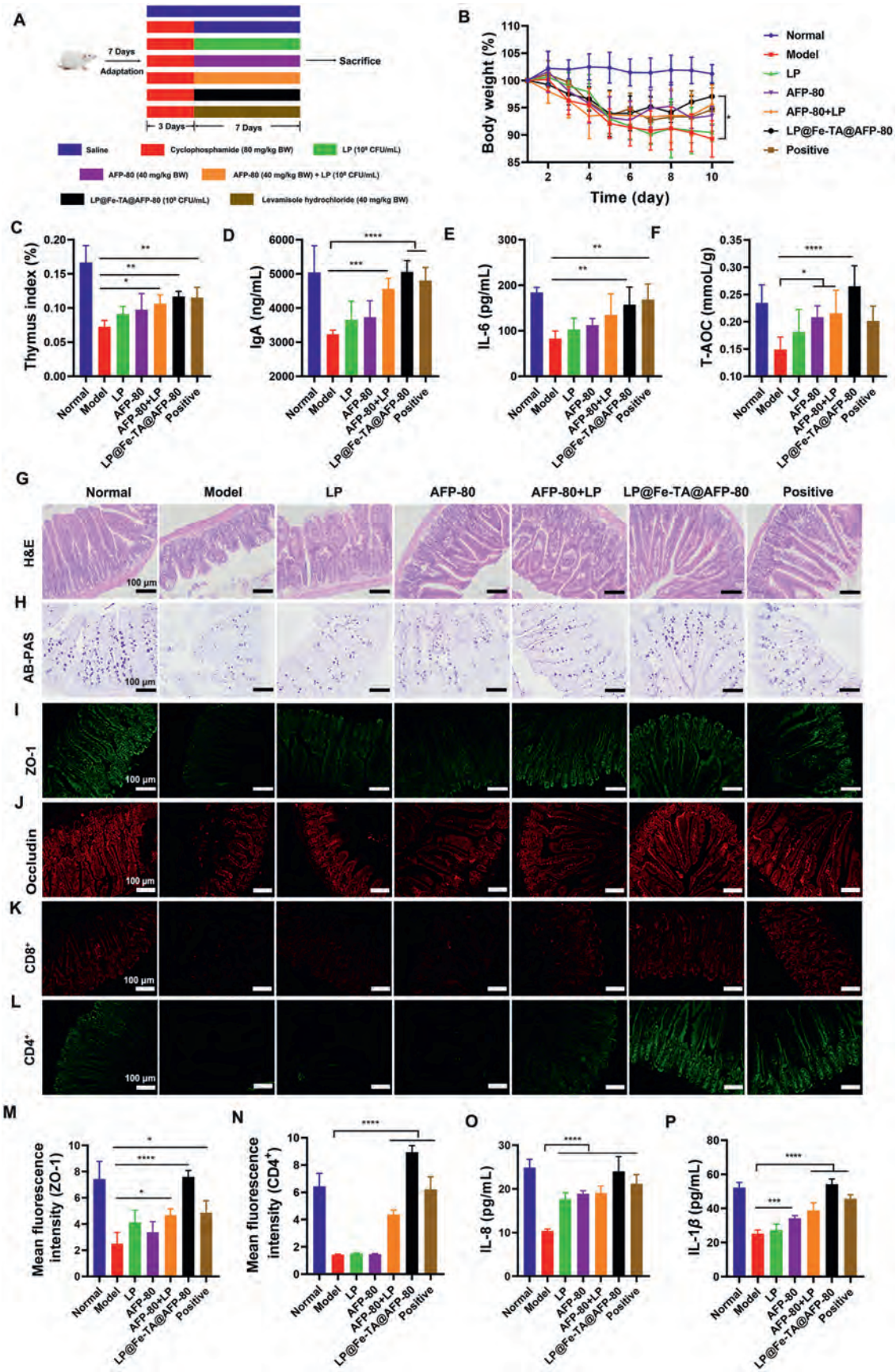
A
7 Days
Adaptation
Sacrifice
3 Days
7 Days
Saline
Cyclophosphamide (80 mg/kg BW)
LP (10⁸ CFU/mL)
AFP-80 (40 mg/kg BW)
AFP-80 (40 mg/kg BW) + LP (10⁸ CFU/mL)
LP@Fe-TA@AFP-80 (10⁸ CFU/mL)
Levamisole hydrochloride (40 mg/kg BW)
B
Body weight (%)
Time (day)
Normal
Model
LP
AFP-80
AFP-80+LP
LP@Fe-TA@AFP-80
Positive
C
Thymus index (%)
D
IgA (ng/mL)
E
IL-6 (pg/mL)
F
T-AOC (mmoL/g)
G
Normal
Model
LP
AFP-80
AFP-80+LP
LP@Fe-TA@AFP-80
Positive
H&E
H
AB-PAS
I
ZO-1
J
Occludin
K
CD8⁺
L
CD4⁺
100 μm
M
Mean fluorescence intensity (ZO-1)
N
Mean fluorescence intensity (CD4⁺)
O
IL-8 (pg/mL)
P
IL-1β (pg/mL)

of incubation. For naive LP and LP@Fe-TA, the viable bacterial number decreased from 7.10 log CFU/mL to 5.26 log CFU/mL, and from 6.78 log CFU/mL to 5.32 log CFU/mL after 3 h of incubation with 4% bile salts, respectively. Whereas, encapsulation of LP with AFP-80 greatly improved their resistance to bile salts (Fig. 3J). This superior protection was further verified visually *via* live/dead bacterial staining (Supporting Information Fig. S20), guaranteeing the premise for LP to exert functions within the body *via* oral consumption. To further investigate whether structural integrity is necessary for protection, AFP-80 was hydrolyzed with trifluoroacetic acid to yield D-AFP-80 for encapsulating LP under the same protocol for fabricating LP@Fe-TA@AFP-80. The results clearly revealed that D-AFP-80 could not protect LP from gastrointestinal stresses due to the loss of the structural integrity (Supporting Information Fig. S21). Eventually, the stability of LP@Fe-TA@AFP-80 in solutions that mimicked entire gastrointestinal conditions (*i.e.*, 2 h exposure in SGF followed by 1 h exposure in SIF [see methods for detailed formula]) was investigated. It was found that the survival amounts of LP@Fe-TA@AFP-80 could still reach 3.33 log CFU/mL after experiencing the simulated whole gastrointestinal conditions, leading to an impressive enhancement of survival in a striking contrast to all death for naive LP (Supporting Information Fig. S22).

Given the universal adhesive capacity of Fe−TA toward various substances (*e.g.*, proteins, RNA, DNA, and small molecules) by forming noncovalent interactions[56], we subsequently examined the potential for Fe−TA to prolong intestinal retention of LP, which is crucial for LP to exert beneficial effects[57]. To elucidate the *in vivo* retention behavior of LP@Fe-TA@AFP-80, two groups of mice received oral administration of Cy5-labeled LP and Cy5-labeled LP@Fe-TA@AFP-80, respectively (see methods for the detailed labeling process). Notably, compared with LP, LP@Fe-TA@AFP-80 exhibited significantly stronger fluorescence within the digestive tract at all detection time points, reaching as high as 3.21 times at 8 h post administration (Fig. 3K and L, Supporting Information Fig. S23). This enhancement should be attributed to the extensive, network-like hydrogen bonding formed between the catechol groups of TA and carbonyl (C═O), amino ($-NH_2$), and imino (−NH−) groups present in mucin, which reinforces adhesion to the intestinal epithelium[58].

3.4. Systematic evaluation of biocompatibility of LP@Fe-TA@AFP-80

Superior biocompatibility is a prerequisite for LP@Fe-TA@AFP-80 to be applied for *in vivo* applications and to be potentially implemented into clinical and people's daily practices. The Fe−TA network is composed of polyphenols and iron ions, both of which have been shown to possess favorable biocompatibility[59]. Additionally, both LP and AFP-80 are derived from food-based sources. Therefore, LP@Fe-TA@AFP-80 was expected to exhibit superior biocompatibility. To assess this, we systematically conducted acute, sub-acute, and long-term biotoxicity studies (Fig. 4A).

For the acute biotoxicity study, according to the instruction of the Organization for Economic Cooperation and Development (OECD) guideline 425 (the guidance for assessing components' impacts on human health and wildlife[40]) a single administration of 200 μL of saline (normal group) or LP@Fe-TA@AFP-80 suspension (1×10^{12} CFU/mL, equivalent to 9.5×10^{13} CFUs per person with an average 60 kg weight, which was 31,600 to 950,000 times higher than the suggested human dose range of 1×10^8 to 3×10^9 CFUs[60], denoted as the high-dose group) was administered to normal mice, followed by monitoring for 14 days and subjection to sacrifice for detailed analysis. No toxic symptoms and statistically significant difference in the body weight were observed during the entire experimental period (Fig. 4B). As expected, the high-dose administration of LP@Fe-TA@AFP-80 demonstrated no significant impacts on organ indices ($P > 0.05$, Fig. 4C, and Supporting Information Fig. S24). Furthermore, serum biochemical indices, including liver function indicators of ALT, AST, and T-BIL, LDH (play a crucial role in the body's energy metabolism process), and kidney function indicators of creatinine (CR), urea, and UA, of mice from the normal group were comparable to those given high concentrations of LP@Fe-TA@AFP-80 (Fig. 4D−F, Supporting Information Fig. S25). Additionally, H&E staining images did not reveal any discernible aberrations, disruption of normal tissue architectures, or signs of inflammation in major organs harvested from both the normal group and the LP@Fe-TA@AFP-80 group (Fig. 4G, Supporting Information Fig. S26). In consideration of the involvement of Fe^{3+} within LP@Fe-TA@AFP-80 and the concomitant accumulation of reactive oxygen species (ROS) during ferroptosis[61], the ROS levels in the spleen, liver, intestine, and thymus were then profiled. As depicted in Supporting Information Fig. S27, the ROS fluorescence intensities of mouse organs harvested from the LP@Fe-TA@AFP-80 group were equivalent to those detected in the normal group.

In accordance with the OECD Test Guidelines 407, a sub-acute biotoxicity study was conducted[42]. One group of mice received oral administration of saline, designated as the normal group, while the other two groups of mice were administered LP@Fe-TA@AFP-80 at doses of 1×10^9 CFU/mL (the low-dose group) and 1×10^{10} CFU/mL (the medium-dose group) daily,

Figure 5 Immunomodulatory effects of LP@Fe-TA@AFP-80 on immunocompromised mice. (A) Schematic of treatments to mice. Healthy mice treated with saline from the beginning to the end were served as the normal group. Mice were provided with Cy (80 mg/kg BW) over a period of 3 days to establish the immunocompromised model. The immunocompromised mice categorized into six groups were given saline, AFP-80, LP, AFP-80 + LP, LP@Fe-TA@AFP-80, and LH, respectively, daily for consecutive 7 days. (B) Weight changes of mice from different groups at different time points post administration. (C) Thymus index of mice from different groups. (D) The concentrations of IgA in mice from different groups. (E) The concentrations of IL-6 in the spleens harvested from different groups. (F) T-AOC levels of liver in mice from different groups. (G) Histopathological features of intestines harvested from different groups at the end of treatments. Scale bar: 100 μm. (H) AB-PAS staining of intestines harvested from various groups at the end of treatments. Scale bar: 100 μm. Images representing immunofluorescence staining of (I) ZO-1 and (J) Occludin within intestines from different groups. Scale bar: 100 μm. Representative immunofluorescence staining images to indicate the existence of (K) $CD8^+$ and (L) $CD4^+$ T cells within intestines from various groups. Scale bar: 100 μm. Mean fluorescence density of immunofluorescence-stained (M) ZO-1 and (N) $CD4^+$ T cells. Cytokine levels, *i.e.*, (O) IL-8 and (P) IL-1β, within intestinal tissues from different groups at the end of treatments, as measured by ELISA. Data are presented as mean ± SD, with sample sizes of $n = 5$ for panels B−F, O, and P; $n = 3$ for panels M and N. Statistical analysis was conducted using either one-way analysis of variance (ANOVA) analysis or Student's *t* test. Significance levels were denoted as follows: $^*P < 0.05$, $^{**}P < 0.01$, $^{***}P < 0.001$, and $^{****}P < 0.0001$.

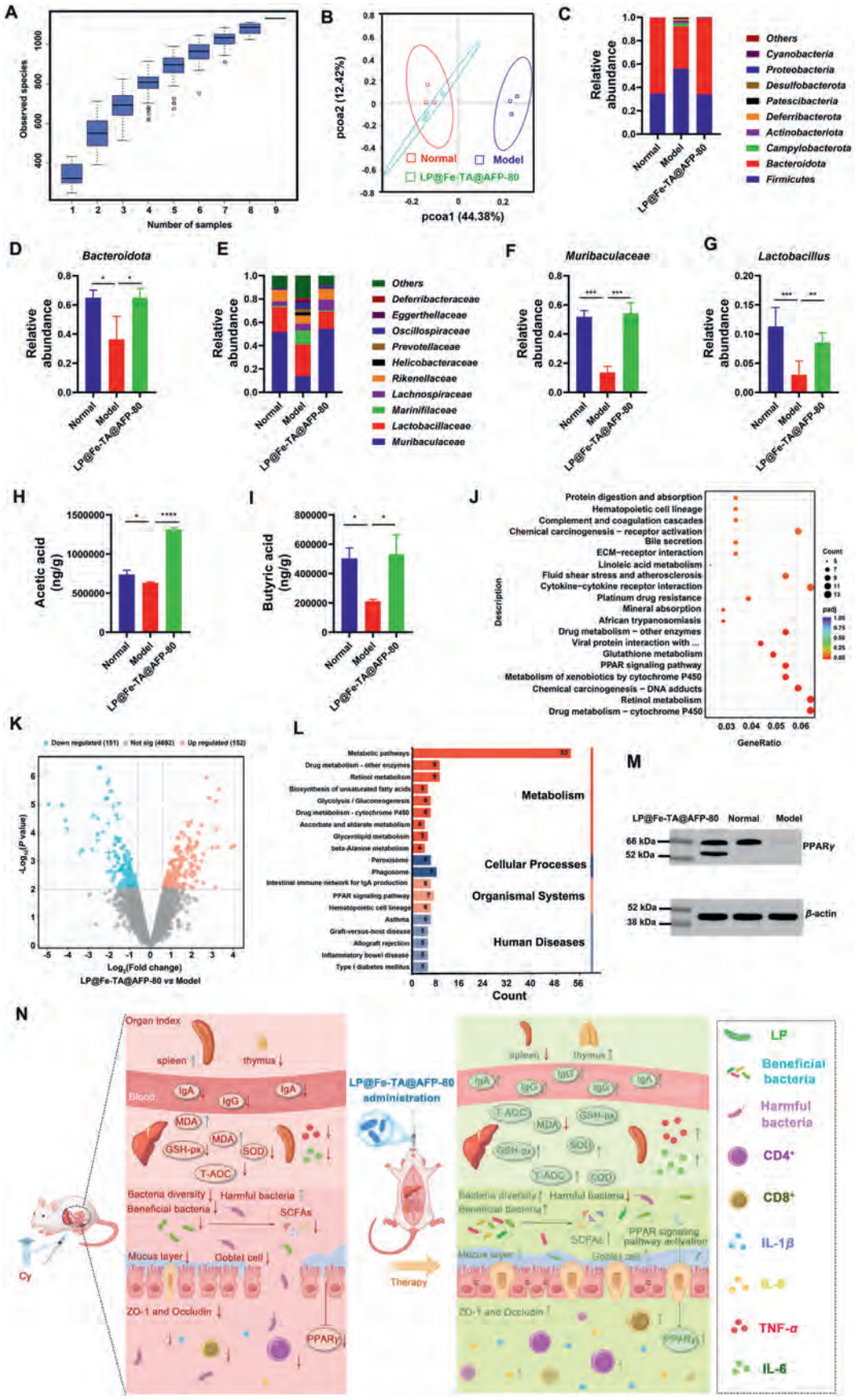
A
Observed species
Number of samples
B
pcoa2 (12.42%)
pcoa1 (44.38%)
Normal
Model
LP@Fe-TA@AFP-80
C
Relative abundance
Others
Cyanobacteria
Proteobacteria
Desulfobacterota
Patescibacteria
Deferribacterota
Actinobacteriota
Campylobacterota
Bacteroidota
Firmicutes
D
Bacteroidota
E
Others
Deferribacteraceae
Eggerthellaceae
Oscillospiraceae
Prevotellaceae
Helicobacteraceae
Rikenellaceae
Lachnospiraceae
Marinifilaceae
Lactobacillaceae
Muribaculaceae
F
Muribaculaceae
G
Lactobacillus
H
Acetic acid (ng/g)
I
Butyric acid (ng/g)
J
Protein digestion and absorption
Hematopoietic cell lineage
Complement and coagulation cascades
Chemical carcinogenesis − receptor activation
Bile secretion
ECM−receptor interaction
Linoleic acid metabolism
Fluid shear stress and atherosclerosis
Cytokine−cytokine receptor interaction
Platinum drug resistance
Mineral absorption
African trypanosomiasis
Drug metabolism − other enzymes
Viral protein interaction with ...
Glutathione metabolism
PPAR signaling pathway
Metabolism of xenobiotics by cytochrome P450
Chemical carcinogenesis − DNA adducts
Retinol metabolism
Drug metabolism − cytochrome P450
Description
GeneRatio
Count
padj
K
Down regulated (151)
Not sig (4692)
Up regulated (152)
-Log10(P value)
Log2(Fold change)
LP@Fe-TA@AFP-80 vs Model
L
Metabolic pathways
Drug metabolism - other enzymes
Retinol metabolism
Biosynthesis of unsaturated fatty acids
Glycolysis / Gluconeogenesis
Drug metabolism - cytochrome P450
Ascorbate and aldarate metabolism
Glycerolipid metabolism
beta-Alanine metabolism
Peroxisome
Phagosome
Intestinal immune network for IgA production
PPAR signaling pathway
Hematopoietic cell lineage
Asthma
Graft-versus-host disease
Allograft rejection
Inflammatory bowel disease
Type I diabetes mellitus
Metabolism
Cellular Processes
Organismal Systems
Human Diseases
Count
M
LP@Fe-TA@AFP-80
Normal
Model
66 kDa
52 kDa
PPARγ
52 kDa
38 kDa
β-actin
N
Organ index
spleen
thymus
Blood
IgA
IgG
MDA
GSH-px
SOD
T-AOC
Bacteria diversity
Harmful bacteria
Beneficial bacteria
SCFAs
Mucus layer
Goblet cell
ZO-1 and Occludin
PPARγ
Cy
LP@Fe-TA@AFP-80 administration
Therapy
PPAR signaling pathway activation
LP
Beneficial bacteria
Harmful bacteria
CD4+
CD8+
IL-1β
IL-6
TNF-α
IL-6

respectively, over a period of 28 days. Clinical observations revealed no signs of treatment-related toxicity. Interestingly, mice in the medium-dose group revealed a weight gain as a function of time, possibly due to enhanced nutrient absorption mediated by LP, similar to the phenomenon observed in previous research[62]. Delightfully, the evaluation of body weight variation and organ indices among all mice didn't show significant differences, which was similar to the case of blood biochemical index investigation (Fig. 4H−K, Supporting Information Figs. S28 and S29). H&E results further confirmed the negligible damages to major organs conferred by consecutive administration of LP@Fe-TA@AFP-80 with different concentrations (Fig. 4L, Supporting Information Fig. S30).

Eventually, we moved to the long-term biotoxicity study. During continuous administration of LP@Fe-TA@AFP-80 (1×10^8 CFU/mL) every 2 days for 6 months, there were no mouse death and abnormal behaviors observed. Correspondingly, negligible adverse impacts toward body weight variation, organ indices (Fig. 4M and N, Supporting Information Figs. S31 and S32), serum biochemistry indices (Fig. 4O and P, Supporting Information Fig. S33), and histopathological morphologies of tissues (Supporting Information Fig. S34) were found by the long-term administration of LP@Fe-TA@AFP-80. Moreover, no over-accumulation of ROS was detected in major organs (Supporting Information Fig. S35).

To further confirm the biosafety profile of LP@Fe-TA@AFP-80, we evaluated the potential for iron accumulation within the body after a 14-day administration. Mice were orally gavaged daily with either saline (denoted as normal group) or LP@Fe-TA@AFP-80 (1×10^8 CFU/mL, denoted as LP@Fe-TA@AFP-80 group). Measurements of total iron contents and transferrin receptor 1 (*TfR1*) expression, an important indicator of iron poisoning[63], in the livers and kidneys showed negligible differences between the two groups (Supporting Information Fig. S36), ruling out the risk of chronic iron poisoning. Moreover, the exogenous supplementation with LP@Fe-TA@AFP-80 did not disrupt the intrinsic microbial balance but rather promoted a favorable shift in the gut microbiota toward a health-associated profile, reinforcing the excellent biocompatibility of LP@Fe-TA@AFP-80 (Supporting Information Fig. S37). According to the body surface area normalization method[64], our applied 1×10^8 CFU/mL dose administered to mice is approximately equivalent to 1.2×10^9 CFU for an adult with an average 70 kg weight. This equivalent dosage exceeds the minimum count (1×10^6 to 1×10^8 CFU) typically required for probiotics to demonstrate functional efficacy in commercial products[65], fully supporting the potential that the LP@Fe-TA@AFP-80 applied under such a dosage can be translated to human to bring therapeutic benefits while refraining from exhibiting biotoxicity. Taken together, all results strongly evidenced that LP@Fe-TA@AFP-80 demonstrated excellent biocompatibility, making it a more suitable candidate for disease treatment or even health management compared to conventional probiotic delivery systems, especially those utilize synthetic polymers, of which the biocompatibility remains insufficiently validated due to their unnatural attributes.

3.5. LP@Fe-TA@AFP-80 efficiently strengthened the immunity in immunocompromised mice

In consideration that the development and progression of various diseases are strongly associated with deficient body immunity, we employed Cy to induce an immunocompromised state in mice to evaluate the immunostimulatory capability of LP@Fe-TA@AFP-80 *in vivo*. Specifically, Cy would inevitably impede the proliferation of effector T cells and promote the proliferation of regulatory T cells (Tregs), correspondingly diminishing the pro-inflammatory cytokine secretion, which promotes the development of immune suppression within the organism[66,67]. According to previous studies[68], an immunocompromised mouse model was established by intraperitoneal injection of 80 mg/kg body weight (BW) Cy daily for 3 consecutive days, followed by oral administration of saline (the model group), AFP-80, LP, the mixture of AFP-80 and LP (the AFP-80 + LP group), LP@Fe-TA@AFP-80, or LH (an immune enhancer that has been applied in the cancer treatment but would cause serious side effects like dizziness and vomiting; the positive group), to parallelly assess their immunostimulatory effects (Fig. 5A). The normal mice administrated with saline throughout the experimental period were designated as the normal group. As illustrated in Fig. 5B, once administrated with Cy, the body weight of mice gradually dropped, particularly on the 4th day in all experimental groups. After different treatments starting from the 4th day, except for those from the normal and model groups, mice in all other experimental groups exhibited a progressive increase in the body weight. Compared to the model group, treatments with AFP-80 + LP or LP@Fe-TA@AFP-80 significantly increased the thymus index while decreasing the spleen index (Fig. 5C and Supporting Information Fig. S38). Notably, the recovery effect on organ indices observed after LP@Fe-TA@AFP-80 treatment was comparable to that of the positive control group.

Furthermore, as revealed in Fig. 5D and Supporting Information Fig. S39, LP@Fe-TA@AFP-80 treatment significantly promoted the secretion of crucial proteins involved in immune

Figure 6 Underlying mechanism of LP@Fe-TA@AFP-80 in strengthening the immunity. (A) Examination of the microbial community through a species accumulation boxplot. (B) β-Diversity was assessed using PCoA based on the unweighted uniFrac distance. (C) Relative abundance of the top 10 phylum of gut microbiota across various groups. (D) Relative abundance of *Bacteroidoota* in different groups. (E) Relative abundance of the top 10 family of gut microbiota in different groups. Relative abundance of (F) *Muribaculaceae* and (G) *Lactobacillus* in different groups. Analysis of SCFAs contents in the colons harvested from different groups, including (H) acetic acid and (I) butyric acid. (J) Bubble diagram of KEGG enrichment of the DEGs between LP@Fe-TA@AFP-80 and model groups. The top 20 most enriched signaling pathways were shown in the bubble diagram. (K) Volcano plot for differentially expressed proteins between LP@Fe-TA@AFP-80 group and model group based on proteomics analysis (P value < 0.01, $|\log_2(\text{Fold Change})| > \log_2(1.5)$). (L) The histogram of KEGG enrichment of the differentially expressed proteins between LP@Fe-TA@AFP-80 and model groups. The top 20 most enriched signaling pathways were shown in the histogram. (M) Western blot analysis of the expression of PPARγ. (N) Schematic diagram of the regulatory mechanism of LP@Fe-TA@AFP-80 on immunocompromised mice. Data are presented as mean ± SD ($n = 3$). Statistical comparisons were conducted using either one-way analysis of variance (ANOVA) analysis or Student's t test. Significance levels were denoted as follows: $^*P < 0.05$, $^{**}P < 0.01$, $^{***}P < 0.001$, and $^{****}P < 0.0001$.

protection, *i.e.*, IgA and IgG. Such promotion led to an increase of 56% and 94%, respectively, in comparison with those in the model group, even surpassing the positive group and approaching levels observed in the normal group. These results underscored the superior immune suppression reinstatement potential of LP@Fe-TA@AFP-80. Specifically, in the case of naive LP, their susceptibility to harsh gastrointestinal stresses impeded their abilities to fully invoke immunoregulatory effects. Compared with either LP or AFP-80 alone, the synergistic effect of AFP-80 and LP led to significant promotion of IgG and IgA secretion as observed in the AFP-80 + LP group, albeit still lower than LP@Fe-TA@AFP-80. The presence of AFP-80 as a protective "shield" within LP@Fe-TA@AFP-80 should account for the above observed results, which led to higher amounts of living LP colonizing within the intestine as characterized above (Fig. 3F−J) to synergize with AFP-80 for a better outcome. Moreover, Cy treatment significantly attenuated the production of IL-6 (Fig. 5E) and TNF-α (Supporting Information Fig. S40) in the spleen. As anticipated, oral administration of LP@Fe-TA@AFP-80 led to a significant elevation of IL-6 levels, which was comparable to that measured in the positive group. The secretion of TNF-α was also enhanced after intervention by AFP-80 + LP or LP@Fe-TA@AFP-80 (Fig. S40), with LP@Fe-TA@AFP-80 still exhibiting the strongest promotion. Numerous studies have demonstrated a correlation between aberrant immune responses and oxidative stress, as the latter would result in a decline in immune cell functions[69]. Since Cy could be metabolized to toxic MDA to induce the oxidative stress, we thus investigated the effect of different treatments on modulating the levels of SOD and GSH-px, two antioxidant enzymes that were crucial for protecting cells against the oxidative stress, and determined the levels of MDA and T-AOC in mice[70]. As illustrated in Supporting Information Fig. S41, the model group exhibited a substantial elevation in MDA levels when compared to the normal group ($P = 0.0012$). Conversely, the administration of AFP-80 + LP ($P = 0.0228$) or LP@Fe-TA@AFP-80 ($P = 0.0022$) resulted in a notable reduction in MDA levels, with LP@Fe-TA@AFP-80 demonstrating superior efficacy. For SOD, GSH-px, and T-AOC, different treatments could positively regulate their levels to some extent, among which LP@Fe-TA@AFP-80 treatment showed the greatest improvement, achieving an increase of 1.44, 4.06, and 1.78 times, respectively, when compared to the model group (Supporting Information Fig. S42 and Fig. 5F).

Given the fact that the intestine is the largest immune organ in the body, we subsequently investigated the regulatory effects of LP, AFP-80, AFP-80 + LP, or LP@Fe-TA@AFP-80 on the intestine in Cy-induced immunocompromised mice. Histological analysis based on H&E staining (Fig. 5G) and Periodic acid Schiff (PAS)−Alcian blue (AB) staining (Fig. 5H) revealed significant intestinal mucosal injury in the model group in comparison with the normal group, characterized by obvious villi atrophy and edema, disordered structures, and the reduced number of goblet cells. Treatment with LP, AFP-80, AFP-80 + LP, or LP@Fe-TA@AFP-80 alleviated intestinal mucosal injury to varying degrees. Particularly, the most notable therapeutic effect was still observed in the LP@Fe-TA@AFP-80 group, leading to the formation of well-structured and densely packed villi, along with an increased abundance of goblet cells, which was consistent with above data of humoral immunity. This structural restoration will ultimately improve nutrient absorption and enhance resistance against bacterial pathogens to benefit the immunity. Subsequently, the expression levels of ZO-1 (Fig. 5I) and Occludin (Fig. 5J), two tight junction proteins, were assessed to evaluate the integrity of the intestinal barrier. Evidently, after being treated with LP, AFP-80, AFP-80 + LP, or LP@Fe-TA@AFP-80, the expression of ZO-1 and Occludin in intestine tissues were increased to varying degrees (Fig. 5M and Supporting Information Fig. S43). In particular, LP@Fe-TA@AFP-80 still demonstrated the most prominent effects on recovering the damage to the intestinal mucosal barrier. Given the crucial role of $CD4^+$ and $CD8^+$ T cells in maintaining intestinal immune homeostasis, we then profiled the T cells across different experimental groups by immunofluorescence staining. As depicted in Fig. 5K and L, intraperitoneal Cy resulted in a significant number reduction of $CD8^+$ and $CD4^+$ T cells in the intestinal tissues, which accounted for only 43.67% and 22.18%, respectively, compared to those observed in the normal group (Supporting Information Fig. S44A and Fig. 5N). Conversely, LP@Fe-TA@AFP-80 treatment remarkably increased $CD8^+$ and $CD4^+$ T cells by approximately 133.61% and 528.87%, respectively, compared to those in the model group. These results were corroborated by flow cytometry (Fig. S44B). In line with this, LP@Fe-TA@AFP-80 treatment led to a secreted enhancement of interleukin-8 (IL-8) and interleukin-1β (IL-1β), two important pro-inflammatory cytokines, by 2.31- and 2.14-fold, respectively (Fig. 5O and P). Eventually, to rule out the potential contribution of Fe−TA in LP@Fe-TA@AFP-80 for immune enhancement, we supplemented experiments to investigate whether oral administration of Fe−TA with the amounts equivalent to that in LP@Fe-TA@AFP-80 can regulate the immune responses following the same administration period and frequency adopted in above LP@Fe-TA@AFP-80-enhanced immunity experiments. As illustrated in Supporting Information Fig. S45, there were no significant differences in the levels of serum IgG and intestinal inflammatory factors (IL-8 and IL-1β) among Fe−TA-treated immunocompromised mice and untreated immunocompromised mice. This finding further supported the conclusion that LP@Fe-TA@AFP-80 achieved a satisfactory immuno-enhancing effect *via* the synergistic effect of living LP and AFP-80.

3.6. In-depth exploration of the immuno-enhancing mechanism of LP@Fe-TA@AFP-80

We further delved into the underlying mechanisms responsible for the enhanced immunomodulatory effects observed in immunocompromised mice achieved by LP@Fe-TA@AFP-80 treatment. It has been well documented that the communications between gut microbiota and the host contribute to maturing the host immune system and modulating the systemic immune responses[71]. Thus, we investigated how LP@Fe-TA@AFP-80 treatment modulated gut microbiota by 16S ribosomal RNA (rRNA) sequencing analysis. After granting sufficient sequencing depth as revealed by species accumulation boxplot analysis (Fig. 6A), the Simpson index was employed to assess the α-diversity of gut microbiota (Supporting Information Fig. S46A). The Simpson index revealed a significant reduction in the α-diversity of gut microbiota in mice treated with Cy ($P = 0.0362$) when compared to the normal group, attributed to the disruption of intestinal tight junctions by Cy, resulting in the translocation of gut microbiota and the facilitation of the invasion of pathogenic microorganisms[72]. However, the LP@Fe-TA@AFP-80 group exhibited a substantial increase in the Simpson index ($P = 0.0319$) compared to the model group. In addition, the Principal Coordinates Analysis (PCoA) revealed significant variations in the β-diversity of gut microbiota between the normal and model groups (Fig. 6B). The microbial community

structure in the LP@Fe-TA@AFP-80 group, however, exhibited a closer resemblance to that of the normal group, which suggested that LP@Fe-TA@AFP-80 was effective in renovating the dysbiosis of gut microbiota in immunocompromised mice. Digging deep, the changes in bacterial compositions of the normal group, model group, and LP@Fe-TA@AFP-80 group were compared at the levels of phylum, family, and genus, respectively. At the phylum level (Fig. 6C), there was a notable decrease in the abundance of *Bacteroidota*, which is a probiotic involved in activating T-cell-mediated responses through interactions with the immune system[73], in the model group ($P = 0.0326$), whereas LP@Fe-TA@AFP-80 markedly enriched *Bacteroidota* abundance to the normal state (Fig. 6D), along with a notable increase in the *Bacteroidota* to *Firmicutes* (B/F) ratio ($P = 0.0438$, Fig. S46B). At the family level (Fig. 6E), mice treated with Cy exhibited a significantly decreased abundance of *Muribaculaceae* ($P = 0.0003$) known to be beneficial bacteria involved in modulating both innate and adaptive immune responses through IgA coating[74], whereas the administration of LP@Fe-TA@AFP-80 effectively reversed this decline (Fig. 6F, $P = 0.0002$). Moreover, the administration of LP@Fe-TA@AFP-80 resulted in a significant reduction in the abundance of *Marinifilaceae* (Fig. S46C, $P = 0.0063$), a kind of bacteria frequently related to gut microbiota dysbiosis and damage to the intestinal barrier[75]. At the genus level (Fig. S46D), *Lactobacillus*, a category of well-studied probiotics that play a critical role in preserving healthy homeostasis[76], showed a 2.83-fold abundance increase in the LP@Fe-TA@AFP-80 group compared to the model group (Fig. 6G). Reports have demonstrated that *Lactobacillus* species contribute positively to the management of various diseases by producing immunomodulatory and antimicrobial compounds that dampen inflammation and help maintain the mucosal barrier[77]. Additionally, *Candidatus_Saccharimonas*, harmful bacteria which can inhibit the production of TNF in macrophages and possess immunosuppressive capabilities, were highly enriched in the gut of immunocompromised mice but were decreased after LP@Fe-TA@AFP-80 treatment (Fig. S46E)[78]. Furthermore, to confirm that the full immunoregulatory effects of LP@Fe-TA@AFP-80 depend critically on the presence of gut microbiota, we established a pseudo-germ-free mouse model by depleting intestinal microorganisms using a broad-spectrum antibiotic cocktail comprising amphotericin B, ampicillin, vancomycin, neomycin sulfate, and metronidazole. Briefly, mice were administered the antibiotic solution for 14 consecutive days, followed by induction of immunosuppression with Cy for 3 days, and subsequently treated with LP@Fe-TA@AFP-80 *via* oral gavage (designated as the A-LP@Fe-TA@AFP-80 group). In parallel, another group of mice received saline instead of antibiotics but underwent the same Cy and LP@Fe-TA@AFP-80 treatment regimen (designated as the LP@Fe-TA@AFP-80 group). Notably, the immunoregulatory efficacy of LP@Fe-TA@AFP-80 against Cy-induced immunosuppression was significantly abolished in the A-LP@Fe-TA@AFP-80 group compared to the LP@Fe-TA@AFP-80 group, as evidenced by aggravated body weight loss (Fig. S47B), severe thymic atrophy (Fig. S47C), and impaired inflammatory (Fig. S47D and S47E) and barrier repair responses (Fig. S47F and S47G). These results collectively demonstrated LP@Fe-TA@AFP-80 exerted a positive regulatory effect on gut microbiota, thus strengthening the immunity of immunocompromised mice.

Short-chain fatty acids (SCFAs), essential metabolites produced by gut microbiota, play a significant role in maintaining individual health and in regulating immune responses[79]. To investigate the impact of LP@Fe-TA@AFP-80 on the production of SCFAs, GC−MS analysis was conducted. The mass concentrations of SCFAs within the gut of mice decreased after the administration of Cy, particularly for acetic acid ($P = 0.0213$), which were significantly lower than those observed in the normal group (Fig. 6H). After administration of LP@Fe-TA@AFP-80, a significant increase in acetic acid levels was observed in immunocompromised mice ($P < 0.0001$). Worth mentioning, acetic acid plays a role in regulating intestinal inflammation by activating G protein-coupled receptor 43 (GPR43) and contributes to maintaining the intestinal epithelial barrier function[80]. As shown in Fig. 6I, the concentration of butyric acid known to aid in dendritic cell differentiation and be closely related to epithelial cell growth significantly increased in the LP@Fe-TA@AFP-80 group compared to the model group ($P = 0.0101$)[81].

RNA sequencing and proteomics analysis were then performed on the gut of mice from both the model group and LP@Fe-TA@AFP-80 group, aiming to further elucidate the underlying immuno-enhancing effect of LP@Fe-TA@AFP-80. A total of 463 differentially expressed genes (DEGs) were detected between the LP@Fe-TA@AFP-80 group and the model group, comprising 269 up-regulated and 194 down-regulated genes (Supporting Information Fig. S48). Furthermore, KEGG analysis revealed that the DEGs were implicated in 255 pathways and the top 20 enriched pathways for DEGs were highlighted in Fig. 6J, prominently featuring signaling pathways like PPAR. Additionally, the proteomics results revealed that, in comparison to the model group, there was a significant up-regulation of 152 proteins and down-regulation of 151 proteins in the LP@Fe-TA@AFP-80 group (Fig. 6K). According to the GO enrichment analysis of up-regulated proteins (Supporting Information Fig. S49), the top-level biological processes happening after intervention by LP@Fe-TA@AFP-80 were "positive regulation of T cell activation", "positive regulation of immune response", and "response to xenobiotic stimulus". Moreover, the KEGG enrichment analysis unveiled that the differentially expressed proteins were implicated in 50 key pathways, and the top 20 up-regulated pathways were displayed in Fig. 6L. Among them, the terms "intestinal immune network for IgA production" classified under the category of "organismal systems" echoed above finding that the amount of IgA increased after LP@Fe-TA@AFP-80 intervention (Fig. 5D), rendering this category more reliable. Besides, a significant enrichment of the PPAR signaling pathway was also identified in this category. Previous studies have highlighted the critical role of the PPAR signaling pathway in immune regulation[82,83]. For instance, in triple-negative breast cancer (TNBC) model, the activation of the PPAR singnaling pathway was positively correlated with the infiltration of classical anti-tumor immune cells, including dendritic cells and M1 macrophages, as well as with the expression of anti-tumor immune-related molecules, which implied a role of PPAR signaling pathway in promoting anti-tumor immunity[84]. Moreover, inhibiting PPARγ (a key member of the PPAR signaling pathway) in myeloid-lineage cells may trigger immunosuppression and tumorigenesis[85]. Furthermore, existing evidence indicates a bidirectional interaction between PPARγ and the gut microbiota. Specifically, the up-regulation of PPARγ can limit gut lumen oxygen level by driving β-oxidation in colonic epithelial cells, thereby inhibiting the expansion of pathogenic Enterobacteriaceae[86]. Conversely, an increase in *Bacteroidota* abundance and its associated metabolite butyrate can activate the PPAR signaling pathway[87]. Given these previous

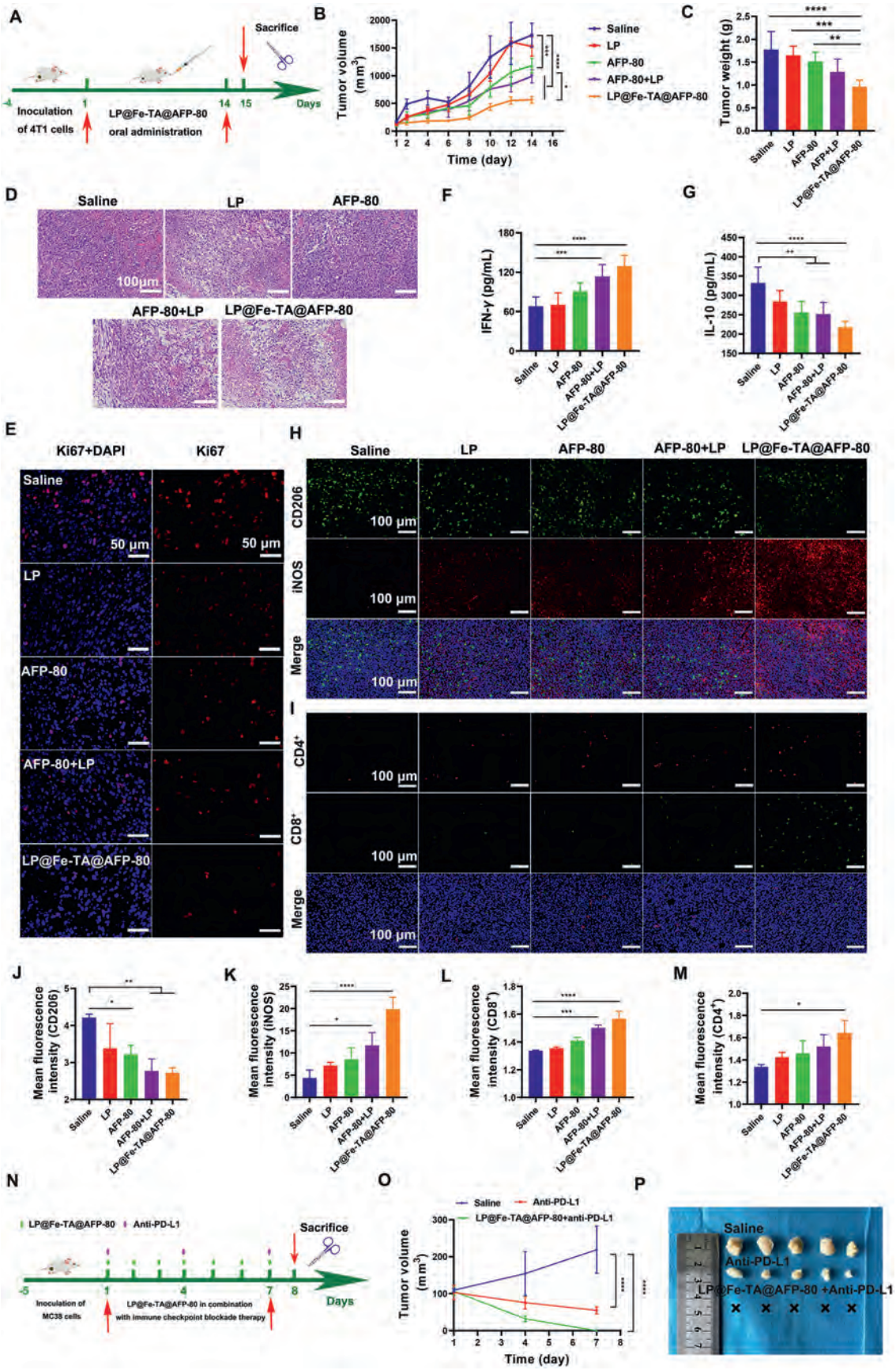
A
Sacrifice
-4
1
14
15
Days
Inoculation of 4T1 cells
LP@Fe-TA@AFP-80 oral administration
B
Tumor volume (mm3)
Time (day)
Saline
LP
AFP-80
AFP-80+LP
LP@Fe-TA@AFP-80
C
Tumor weight (g)
D
Saline
LP
AFP-80
AFP-80+LP
LP@Fe-TA@AFP-80
100μm
F
IFN-γ (pg/mL)
G
IL-10 (pg/mL)
E
Ki67+DAPI
Ki67
50 μm
H
CD206
iNOS
Merge
100 μm
I
CD4+
CD8+
J
Mean fluorescence intensity (CD206)
K
Mean fluorescence intensity (iNOS)
L
Mean fluorescence intensity (CD8+)
M
Mean fluorescence intensity (CD4+)
N
LP@Fe-TA@AFP-80
Anti-PD-L1
Sacrifice
-5
1
4
7
8
Days
Inoculation of MC38 cells
LP@Fe-TA@AFP-80 in combination with immune checkpoint blockade therapy
O
Saline
Anti-PD-L1
LP@Fe-TA@AFP-80+anti-PD-L1
Tumor volume (mm3)
Time (day)
P
Saline
Anti-PD-L1
LP@Fe-TA@AFP-80 +Anti-PD-L1

findings, we further investigated the expression of PPARγ in the gut of mice across different groups to ascertain the potential association between the immunomodulatory effects of LP@Fe-TA@AFP-80 and PPAR signaling pathway. As shown in Fig. 6M and Supporting Information Fig. S50, the expression of PPARγ was significantly up-regulated in the LP@Fe-TA@AFP-80 group compared to the model group, underscoring the strong connection between the immune enhancement empowered by LP@Fe-TA@AFP-80 and activation of PPAR signaling pathway. To further investigate this association, a PPARγ inhibitor (GW9662, 1 mg/kg·BW) was administered *via* intraperitoneal injection to immunosuppressed mice followed by LP@Fe-TA@AFP-80 treatment (designated as the GW9662 + LP@Fe-TA@AFP-80 group), and a parallel comparison of the immune recovery status of mice treated with sole LP@Fe-TA@AFP-80 (designated as the LP@Fe-TA@AFP-80 group) (Supporting Information Fig. S51A) was conducted. As shown in Fig. S51, compared with the mice that only received the LP@Fe-TA@AFP-80 treatment, the immune recovery of the mice in the GW9662 + LP@Fe-TA@AFP-80 group was significantly inhibited. Specifically, the GW9662 + LP@Fe-TA@AFP-80 group showed significantly reduced weight gain (Fig. S51B), persistent splenomegaly (Fig. S51C), a significantly smaller thymus (Fig. S51D), and diminished hepatic antioxidant capacity (Fig. S51E and S51F) relative to the LP@Fe-TA@AFP-80 group. Moreover, the inflammatory response of the mice in the GW9662 + LP@Fe-TA@AFP-80 group was significantly weakened, as evidenced by the decreased expression of key inflammatory factors (such as IL-1β and IL-8; Fig. S51G and S51H), and the recovery of the intestinal barrier was also significantly impaired (Fig. S51I and S51J). In summary, these findings confirmed that PPAR signaling pathway activation played a crucial role in mediating the immunomodulatory effect of LP@Fe-TA@AFP-80. In addition, the proteins associated with the "hematopoietic cell lineage" were also found to be significantly up-regulated in the "organismal systems" category. This observation may be attributed to the indirect influence on the mobilization and homing of hematopoietic stem cells (HSCs) due to the immune enhancement regulated through LP@Fe-TA@AFP-80[88]. Furthermore, as found above, LP@Fe-TA@AFP-80 led to an up-regulation in the expression of cytokines in immunocompromised mice, such as TNF-α (Fig. S40), IL-6 (Fig. 5E), and IL-1β (Fig. 5P), which could also impact the quiescence and differentiation of HSCs[89]. Under the category of "Metabolism", we observed a significant up-regulation of proteins associated with "metabolic pathways", indicating a close correlation between the immune restoration in mice and the enhancement of metabolic processes, which will be further investigated in our future research. Collectively, with all these findings, it was deciphered that oral consumption of LP@Fe-TA@AFP-80 can reinstate gut microbiota balance and involve the activation of PPAR signaling pathway, which led to above observed phenomena of positive regulation of humoral/intestinal immunity, restoration of the intestinal barrier, immunostimulatory cytokine-secreted promotion, and enhancement of the body antioxidative ability, thus achieving an efficient immuno-enhancing effect (Fig. 6N).

3.7. LP@Fe-TA@AFP-80 remodeled tumor immune microenvironment and gut microbiota to efficiently combat cancer

Driven by the efficient immuno-enhancing effect *in vivo*, we wondered whether LP@Fe-TA@AFP-80 can be exploited to combat cancer, a worldwide and fatal disease whose occurrence and progression are closely related to body's immune deficiency. To evaluate this, mice bearing 4T1 breast tumors were randomly assigned to 5 groups and were orally administrated with different formulations, including saline, LP, AFP-80, the mixture of AFP-80 and LP, and LP@Fe-TA@AFP-80 (denoted as the saline, LP, AFP-80, AFP-80 + LP, and LP@Fe-TA@AFP-80 group, respectively) from Day 1 to Day 14 (Fig. 7A). The tumor growth curves and tumor weights measured at the end of the intervention indicated that sole LP or AFP-80 mildly inhibited tumor growth due to the suboptimal immuno-enhancing effect as characterized above. Their physical mixture of AFP-80 + LP demonstrated a moderate inhibitory effect on tumor growth (Fig. 7B and C, Supporting Information Fig. S52). Once treated with LP@Fe-TA@AFP-80, the mice exhibited a satisfactory inhibition effect, featuring a significantly higher tumor inhibition rate of 56.08%. To further assess the *in vivo* inhibitory effect, H&E staining was performed for the histological examination of tumor tissues. The results revealed that tumor sections collected from the LP@Fe-TA@AFP-80 group exhibited significant nuclear changes, including pyknosis, karyorrhexis, and karyolysis (Fig. 7D). Consistently, the LP@Fe-TA@AFP-80 group exhibited the least positive staining for Ki67 protein as demonstrated in Fig. 7E and Supporting Information Fig. S53, indicating a notable suppression of cell proliferation. However, direct co-culture of LP@Fe-TA@AFP-80 with 4T1 cells did not induce detectable cytotoxicity, suggesting that its anti-tumor efficacy was not mediated by direct interactions with the cancer cells (Supporting Information Fig. S54).

Cytokines in the serum could coordinate immune responses within the body *via* blood circulation for anti-tumor processes[90].

Figure 7 Oral administration of LP@Fe-TA@AFP-80 for the treatment of tumors. (A) A schematic illustration of the establishment of the 4T1 tumor model and corresponding treatment scenarios. (B) The variation of relative tumor volume as a function of time during treatment period across different groups. (C) Tumor weights in different groups at the end of 4T1 tumor treatment. (D) Representative H&E images of tumor tissues from various treatment groups. Scale bar: 100 μm. (E) Images of immunofluorescence staining for assessing tumor cell proliferation (Ki67). Scale bar: 50 μm. The secretion of serum cytokines of (F) IFN-γ and (G) IL-10 in mice from different treatment groups. (H) Images of immunofluorescence staining for assessing macrophage polarization. CD206 channel corresponds to M2 macrophage and iNOS channel corresponds to M1 macrophage. Scale bar: 100 μm. (I) Images of immunofluorescence staining for assessing T cell infiltration into the tumor (*i.e.*, $CD4^+$ and $CD8^+$). Scale bar: 100 μm. Mean fluorescence density of immunofluorescence-stained (J) CD206, (K) iNOS, (L) $CD8^+$ T cells, and (M) $CD4^+$ T cells. (N) A schematic illustration of the establishment of the MC38 tumor model and corresponding treatment scenarios. (O) The variation of relative tumor volume as a function of time during treatment period across different groups. (P) Digital photo of dissected tumors after different treatments. Data are presented as mean ± SD, with sample sizes of $n = 5$ for panels B, C, F, G, O, and P, and $n = 3$ for panels J−M. Statistical comparisons were conducted using either one-way analysis of variance (ANOVA) analysis or Student's *t* test. Significance levels were denoted as follows: $^*P < 0.05$, $^{**}P < 0.01$, $^{***}P < 0.001$, and $^{****}P < 0.0001$.

To our delight, LP@Fe-TA@AFP-80-treated mice exhibited the most significant variations of IFN-γ (a pro-inflammatory cytokine) and interleukin-10 (IL-10, an anti-inflammatory cytokine) levels in serum compared to those measured in the saline group (Fig. 7F and G), of which the decline of IL-10 with simultaneous elevation of IFN-γ is conducive to enhancing circulating immune system of the host for combating the tumors. To dig deeper, we investigated the mechanism underlying the satisfactory inhibition of tumors achieved by LP@Fe-TA@AFP-80 treatment, with a specific focus on how LP@Fe-TA@AFP-80 regulated tumor immune microenvironment (TIME). Revealed by Supporting Information Fig. S55, the observed concurrent decrease in IL-10 and increase in IFN-γ within the tumor tissues, which followed a similar trend measured in serum, suggested that the immunosuppressive nature of TIME was relieved after LP@Fe-TA@AFP-80 intervention. Considering the fact that tumor-associated macrophages (TAMs) were closely related to the immunosuppressive nature of the tumor microenvironment, their phenotypes were thus profiled using immunofluorescence staining among all experimental groups[91]. The LP@Fe-TA@AFP-80 group showed the most marked decrease in CD206-positive cells, demonstrating a reduction in M2 macrophages that facilitate tumor growth. In contrast, this group exhibited the highest proportion of iNOS-positive cells, characteristic of M1 macrophages known to inhibit tumor growth, indicating the reprogramming of the TIME (Fig. 7H−J and K). Furthermore, it was found that LP@Fe-TA@AFP-80 induced the highest intratumoral infiltration of $CD4^+$ and $CD8^+$ T cells, realizing strong cellular immunity against tumors (Fig. 7I, L and M)[92]. Flow cytometric analysis further confirmed these shifts and revealed enhanced anti-tumor immunity, as evidenced by the shifts in tumor-associated macrophages toward the M1 phenotype in the tumors (Supporting Information Fig. S56), along with an increased abundance of $CD80^+CD86^+$ dendritic cells in both the tumors and spleens (Supporting Information Fig. S57). Thus, orally delivered LP@Fe-TA@AFP-80 achieved potent 4T1 tumor inhibition by effectively remodeling the TIME (Supporting Information Fig. S58). These immune alterations were likely associated with intestinal immune modulation, as shown in our earlier findings (Fig. 5I−P). More specifically, following activation in Peyer's patches, intestinal immune cells can disseminate *via* the lymphatic and circulatory systems, thereby linking mucosal immunity to systemic antitumor responses and contributing to the remodeling of the TIME[93].

Furthermore, 16S rRNA analysis revealed that LP@Fe-TA@AFP-80 supplementation reshaped the gut microbial profile to the one more favorable for anti-tumor purposes (Figs. S59−S63). Specifically, at the phylum levels (Supporting Information Fig. S62A), the abundance of *Proteobacteria*, a kind of bacteria with pathogenicity that impairs anti-tumor immunity by consuming arginine and restoring the suppressive function of adipose-associated Tregs[43,94], increased significantly in the saline group ($P = 0.0321$). Delightfully, oral administration of LP@Fe-TA@AFP-80 led to an abundance decline of *Proteobacteria* to levels similar to those observed in the normal group (normal mice, Fig. S62B). The abundance of *Stenotrophomonas*, harmful bacteria known to be capable of eliciting multiple infections toward immunocompromised individuals for potential tumor induction[95], significantly increased at the genus level in the saline group ($P = 0.0106$) and were correspondingly reduced after the intervention of LP@Fe-TA@AFP-80 (Fig. S63A and S63B, $P = 0.0082$). Additionally, *Streptococcus*, a crucial category of bacteria that can produce cadaverine to exert anti-tumor effects by inhibiting epithelial−mesenchymal transition, cell motility, chemotaxis, and metastasis, were markedly enriched in breast cancer mice after LP@Fe-TA@AFP-80 treatment (Fig. S63C, $P = 0.0195$)[96,97]. In sum, our results demonstrated that the anti-tumor efficacy of LP@Fe-TA@AFP-80 was not attributable to direct cytotoxicity but rather resulted from a multilevel synergistic mechanism involving intestinal immune activation and gut microbiota modulation.

In consideration of the positive regulation of TIME, we were pushed forward to exploit LP@Fe-TA@AFP-80 in combination with immune checkpoint blockade therapy, which has been adopted in clinic practices for preventing the immune escape of tumor cells. Here, the MC38 tumor overexpressing PD-L1, one typical immune checkpoint, was chosen as the model (Fig. 7N). Excitingly, the LP@Fe-TA@AFP-80 plus anti-PD-L1 treatment efficiently reversed the tumor development, which eventually eradicated the tumors, highlighting the great potential of LP@Fe-TA@AFP-80 as a therapeutic in oncology (Fig. 7O and P, Supporting Information Fig. S64).

4. Conclusions

In summary, we developed an oral immune enhancer (LP@Fe-TA@AFP-80) with decent effectiveness and excellent biocompatibility through bridging LP and AFP-80 by Fe−TA adhesive layer. Due to enhanced gastrointestinal resistance of LP contributed by AFP-80 shielding, much more LP survived after oral administration to synergize with AFP-80 for better immune modulation. Excitingly, the oral immune enhancer demonstrated excellent biocompatibility, showing imperceptible biotoxicity in mice even after 6 months' consecutive oral administration, possibly attributed to the fact that the components constructing the immune enhancer were derived from food-based sources. In immunocompromised mice, oral administration of LP@Fe-TA@AFP-80 effectively renovated the immunity by restoring gut microbiota dysbiosis and involving the activation of the PPAR signaling way, featuring ameliorative organ indices, elevated serum levels of immunoglobulins, increased secretion of immunostimulatory cytokines, enhanced body's antioxidative activity, and restoration of intestinal barrier. Additionally, the inhibitory impact of LP@Fe-TA@AFP-80 on tumor progression through remodeling tumor immune microenvironment (*i.e.*, macrophage phenotypical transformation, intratumoral infiltration of $CD4^+$/$CD8^+$ T cells, and positive regulation of immunoregulatory cytokines) and gut microbiota was successfully validated on a 4T1 breast cancer murine model. Excitingly, in combination with anti-PD-L1, LP@Fe-TA@AFP-80 successfully reversed the growth of MC38 tumors in mice, evetually eradicating the tumors. The strategy of exploiting probiotic−polysaccharide complexes for the immuno-enhancing purpose developed here opens an avenue to explore natural substances with high biocompatibility to design and construct oral therapeutic agents demonstrating effective performance for combating diseases.

Undeniably, as an immune enhancer, LP@Fe-TA@AFP-80 warrants further investigation in the future before the possible clinical translation. For example, while the formulation has demonstrated significant therapeutic potentials in mouse models, additional studies using primate models with physiology more closely resembling that of humans (*e.g.*, monkeys) are required. Such studies will allow comprehensive evaluation of pharmacokinetics, biodistribution, long-term safety, and immune regulatory

mechanisms under clinically representative conditions. In parallel, further work is warranted to develop scalable manufacturing processes. In addition, the exploration of the synergistic effects with other clinically-used immune stimulants would highlight the significance of the clinical translation of LP@Fe-TA@AFP-80. Collectively, these efforts will strengthen the foundation for clinical translation.

Acknowledgments

This work was primarily funded by a National Natural Science Foundation of China (No. 32372322). Natural Science Foundation of Jiangxi Province (Nos. 20224ACB215009, 20232ACB205024, and 20242BAB21029, China). China Postdoctoral Science Foundation (No. 2025M773007).

Author contributions

Anqi Xie: Conceptualization, Methodology, Investigation, Formal analysis, Writing original draft, Funding acquisition. Lei Feng: Methodology, Writing - review & editing. Yaping Shao: Methodology, Formal analysis. Yiqun Wan: Methodology. Ying Zhang: Writing original draft, Funding acquisition. Zheyi Liu: Methodology, Investigation. Haihua Ji: Investigation. Hao Wan: Conceptualization, Writing - Review & Editing, Supervision, Funding acquisition, Project administration.

Conflicts of interest

The authors declare no conflicts of interest.

Appendix A. Supporting information

Supporting information to this article can be found online at https://doi.org/10.1016/j.apsb.2026.01.041.

References

1. Wu W, Guo F, Wang C, Qu X, Wang Q, Yang Y, et al. Biomimetic "trojan horse" nanoparticles with biotactic behavior toward tumor-associated bacteria for targeted therapy of colorectal cancer. *Cell Biomater* 2025;**1**:100092.
2. Zhang C, Niu J, Li J, Zhang H, Yu Q, Chen Y, et al. Polysaccharide based supramolecular injectable hydrogels for *in situ* treatment of bladder cancer. *Chin Chem Lett* 2024;**35**:108556.
3. Liu Z, Zhang S, Hu H, Wang H, Qiu Y, Dong M, et al. Construction of recombinant lactococcus expressing thymosin and interferon fusion protein and its application as an immune adjuvant. *Microb Cell Fact* 2024;**23**:1−19.
4. Gutjahr A, Tiraby G, Perouzel E, Verrier B, Paul S. Triggering intracellular receptors for vaccine adjuvantation. *Trends Immunol* 2016;**37**:716.
5. Xiong H, Han X, Cai L, Zheng H. Natural polysaccharides exert anti-tumor effects as dendritic cell immune enhancers. *Front Oncol* 2023; **13**:1274048.
6. Kimani FW, Manna S, Moser B, Shen J, Nihesh N, Esser-Kahn AP. Improving the adjuvanticity of small molecule immune potentiators using covalently linked NF-κB modulators. *ACS Med Chem Lett* 2021; **12**:1441−8.
7. Yu D, Zuo Y, Qi M, Zhong H. Advances in the combination of immunoadjuvants and tumor ablation: mediating immune effects to enhance anti-tumor efficacy. *Biochim Biophys Acta Rev Cancer* 2025; **1880**:189393.
8. Banstola A, Jeong JH, Yook S. Immunoadjuvants for cancer immunotherapy: a review of recent developments. *Acta Biomater* 2020;**114**: 16−30.
9. Wang Y, Gong N, Ma C, Zhang Y, Tan H, Qing G, et al. An amphiphilic dendrimer as a light-activable immunological adjuvant for *in situ* cancer vaccination. *Nat Commun* 2021;**12**:4964.
10. Gu P, Wusiman A, Wang S, Zhang Y, Liu Z, Hu Y, et al. Polyethylenimine-coated PLGA nanoparticles-encapsulated angelica sinensis polysaccharide as an adjuvant to enhance immune responses. *Carbohydr Polym* 2019;**223**:115128.
11. Luo L, Iqbal MZ, Liu C, Xing J, Akakuru OU, Fang Q, et al. Engineered nano-immunopotentiators efficiently promote cancer immunotherapy for inhibiting and preventing lung metastasis of melanoma. *Biomaterials* 2019;**223**:119464.
12. Zhao J, Hu G, Huang Y, Huang Y, Wei X, Shi J. Polysaccharide conjugate vaccine: a kind of vaccine with great development potential. *Chin Chem Lett* 2021;**32**:1331−40.
13. Kozarski M, Klaus A, van Griensven L, Jakovljevic D, Todorovic N, Wan-Mohtar WAAQI, et al. Mushroom β-glucan and polyphenol formulations as natural immunity boosters and balancers: nature of the application. *Food Sci Hum Wellness* 2023;**12**:378−96.
14. Lacaille-Dubois MA. Updated insights into the mechanism of action and clinical profile of the immunoadjuvant QS-21: a review. *Phytomedicine* 2019;**60**:152905.
15. Xu J, Yu Y, Zhang Y, Dai H, Yang Q, Wang B, et al. Oral administration of garlic-derived nanoparticles improves cancer immunotherapy by inducing intestinal IFNγ-producing $\gamma\delta$ T cells. *Nat Nanotechnol* 2024;**19**:1569−78.
16. Dalla Pietà A, Carpanese D, Grigoletto A, Tosi A, Dalla Santa S, Pedersen GK, et al. Hyaluronan is a natural and effective immunological adjuvant for protein-based vaccines. *Cell Mol Immunol* 2021;**18**: 1197−210.
17. Jiang Y, Qi S, Mao C. Polysaccharide nanoparticles as potential immune adjuvants: mechanism and function. *Acta Pharm Sin B* 2025;**15**: 1796−815.
18. Gao Y, Gao Y, Ding Y, Tan H, Zou A, Li S. Polysaccharide-based supramolecular drug delivery systems mediated *via* host−guest interactions of cucurbiturils. *Chin Chem Lett* 2021;**32**: 949−53.
19. Zhao L, Niu M, Ma Z, He F, Liu X, Gong X, et al. Modified probiotics and the related combinatorial therapeutics. *Acta Pharm Sin B* 2025;**15**: 2431−53.
20. Ni D, Qing S, Ding H, Yue H, Yu D, Wang S, et al. Biomimetically engineered demi-bacteria potentiate vaccination against cancer. *Adv Sci* 2017;**4**:1700083.
21. Peñalva R, Martínez-López AL, Gamazo C, Gonzalez-Navarro CJ, González-Ferrero C, Virto-Resano R, et al. Encapsulation of *Lactobacillus plantarum* in casein-chitosan microparticles facilitates the arrival to the colon and develops an immunomodulatory effect. *Food Hydrocoll* 2023;**136**:108213.
22. Li L, Hao J, Jiang Y, Hao P, Gao Y, Chen J, et al. A micro-sized vaccine based on recombinant *Lactiplantibacillus* plantarum fights against SARS-CoV-2 infection *via* intranasal immunization. *Acta Pharm Sin B* 2023;**13**:3168−76.
23. Centurion F, Basit AW, Liu J, Gaisford S, Rahim MA, Kalantar-Zadeh K. Nanoencapsulation for probiotic delivery. *ACS Nano* 2021; **15**:18653−60.
24. Chen X, Zhang Y, Chen T, Ji H, Liu J, Yang L, et al. Implement enhanced artificial "enteroendocrine L cells" *via* oral administration for effective treatment of type 2 diabetes. *Cell Biomater* 2025;**1**: 100024.
25. Yao M, Xie J, Du H, McClements DJ, Xiao H, Li L. Progress in microencapsulation of probiotics: a review. *Compr Rev Food Sci F* 2020;**19**:857−74.
26. Wang Y, Li C, Li J, Zhang S, Zhang Q, Duan J, et al. *Abelmoschus manihot* polysaccharide fortifies intestinal mucus barrier to alleviate intestinal inflammation by modulating *Akkermansia muciniphila* abundance. *Acta Pharm Sin B* 2024;**14**:3901−15.

27. Liu Y, Wu J, Hao H. Antitumor immunostimulatory activity of the traditional Chinese medicine polysaccharide on hepatocellular carcinoma. *Front Immunol* 2024;**15**:1369110.
28. Nguyen TP, Phan HN, Do TD, Do GD, Ngo LH, Do HDK, et al. Polysaccharide and ethanol extracts of *Anoectochilus formosanus* Hayata: antioxidant, wound-healing, antibacterial, and cytotoxic activities. *Heliyon* 2023;**9**:e13559.
29. Ho Y, Chen YF, Wang LH, Hsu KY, Chin YT, Yang YSH, et al. Inhibitory effect of *Anoectochilus formosanus* extract on hyperglycemia-related PD-L1 expression and cancer proliferation. *Front Pharmacol* 2018;**9**:807.
30. Yang LC, Lu TJ, Lin WC. A type II arabinogalactan from *Anoectochilus formosanus* for G-CFS production in macrophages and leukopenia improvement in CT26-bearing mice treated with 5-fluorouracil. *Evid Based Complement Alternat Med* 2013;**2013**:458075.
31. Yang LC, Lai CY, Lin WC. Natural killer cell-mediated cytotoxicity is increased by a type II arabinogalactan from *Anoectochilus formosanus*. *Carbohydr Polym* 2017;**155**:466−74.
32. Wu Y, Liu C, Jiang Y, Bai B, He X, Wang H, et al. Structural characterization and hepatoprotective effects of polysaccharides from *Anoectochilus zhejiangensis*. *Int J Biol Macromol* 2022;**198**:111−8.
33. Xie A, Wan H, Feng L, Yang B, Wan Y. Protective effect of *Anoectochilus formosanus* polysaccharide against cyclophosphamide-induced immunosuppression in BALB/c mice. *Foods* 2023;**12**:1−15.
34. Wang J, Chen X, Chen Y, Qin F, Yang H. Pharmacological effects and mechanisms of tannic acid. *Biomed Pharmacother* 2022;**154**:113561.
35. Shah Bhagwan G, Alexandre Giroux, Belonje B. Specifications for reduced iron as a food additive. *J Agric Food Chem* 1977;**25**:592−4.
36. Xie A, Ji H, Liu Z, Wan Y, Zhang X, Xiong H, et al. Modified prebiotic-based "shield" armed probiotics with enhanced resistance of gastrointestinal stresses and prolonged intestinal retention for synergistic alleviation of colitis. *ACS Nano* 2023;**17**:14775−91.
37. Zhang Z, Guo L, Yan A, Feng L, Wan Y. Fractionation, structure and conformation characterization of polysaccharides from *Anoectochilus roxburghii*. *Carbohydr Polym* 2020;**231**:115688.
38. Feng L, Yin J, Nie S, Wan Y, Xie M. Fractionation, physicochemical property and immunological activity of polysaccharides from *Cassia obtusifolia*. *Int J Biol Macromol* 2016;**91**:946−53.
39. Zhao JY, Hong T, Hou YJ, Song XX, Yin JY, Geng F, et al. Comparison of structures and emulsifying properties between water-extracted pectins from *Fructus aurantii*. *Int J Biol Macromol* 2023;**242**:125005.
40. OECD. *Test no. 425: acute oral toxicity: Up-and-down procedure*. 2022.
41. Pradhan D, Singh R, Tyagi A, R HM, Batish VK, Grover S. Assessing safety of *Lactobacillus plantarum* MTCC 5690 and *Lactobacillus fermentum* MTCC 5689 using *in vitro* approaches and an *in vivo* murine model. *Regul Toxicol Pharmacol* 2019;**101**:1−11.
42. OECD. *Test no. 407: repeated dose 28-day oral toxicity study in rodents*. 2008.
43. Song W, Wang Y, Li G, Xue S, Zhang G, Dang Y, et al. Modulating the gut microbiota is involved in the effect of low-molecular-weight *Glycyrrhiza* polysaccharide on immune function. *Gut Microbes* 2023;**15**:2276814.
44. Pettolino FA, Walsh C, Fincher GB, Bacic A. Determining the polysaccharide composition of plant cell walls. *Nat Protoc* 2012;**7**: 1590−607.
45. Tang W, Li AQ, Yin JY, Nie SP. Structural characteristics of three pectins isolated from white kidney bean. *Int J Biol Macromol* 2021; **182**:2151−61.
46. Lai CY, Yang LC, Lin WC. Type II arabinogalactan from *Anoectochilus formosanus* induced dendritic cell maturation through TLR2 and TLR4. *Phytomedicine* 2015;**22**:1207−14.
47. Yang LC, Lin WC, Lu TJ. Characterization and prebiotic activity of aqueous extract and indigestible polysaccharide from *Anoectochilus formosanus*. *J Agric Food Chem* 2012;**60**:8590−9.
48. Chen S, Saeed AFUH, Liu Q, Jiang Q, Xu H, Xiao GG, et al. Macrophages in immunoregulation and therapeutics. *Signal Transduct Targeted Ther* 2023;**8**:1−35.
49. Wang K, Liu X, Xiao H, Wang H, Zhang Y. The correlation between inflammatory injury induced by lps and ras in EpH4-Ev cells. *Int Immunopharmacol* 2017;**46**:23−30.
50. Palmieri EM, McGinity C, Wink DA, McVicar DW. Nitric oxide in macrophage immunometabolism: hiding in plain sight. *Metabolites* 2020;**10**:429.
51. Park EJ, Lee JH, Yu GY, He G, Ali SR, Holzer RG, et al. Dietary and genetic obesity promote liver inflammation and tumorigenesis by enhancing iL-6 and TNF expression. *Cell* 2010;**140**:197−208.
52. Qin J, Wang H-y, Zhuang D, Meng F-c, Zhang X, Huang H, et al. Structural characterization and immunoregulatory activity of two polysaccharides from the rhizomes of *Atractylodes lancea* (Thunb.) DC. *Int J Biol Macromol* 2019;**136**:341−51.
53. Duan JL, Liu MQ, Liu YN, Liang XF, Cao C, Yao AN, et al. Comparative study on physicochemical characterization and immunomodulatory activities of neutral and acidic *Lycium barbarum* polysaccharides. *Biomed Pharmacother* 2024;**181**:117659.
54. Zhang S, Li P, Lee S, Wang Y, Tan C, Shang N. Weizmannia coagulans: an ideal probiotic for gut health. *Food Sci Hum Wellness* 2023;**13**:1−20.
55. Fang T, Liu S. Metal−phenolic network directed coating of single probiotic cell followed by photoinitiated thiol-ene click fortification to enhance oral therapy. *Small* 2023;**20**:2308146.
56. Guo J, Tardy BL, Christofferson AJ, Dai Y, Richardson JJ, Zhu W, et al. Modular assembly of superstructures from polyphenol-functionalized building blocks. *Nat Nanotechnol* 2016;**11**:1105−11.
57. Liu J, Li W, Wang Y, Ding Y, Lee A, Hu Q. Biomaterials coating for on-demand bacteria delivery: selective release, adhesion, and detachment. *Nano Today* 2021;**41**:101291.
58. Tang Z, Huang Z, Huang Y, Huang M, Liu H, Du J, et al. Nanomedicine's shining armor: understanding and leveraging the metal−phenolic networks. *J Nanobiotechnol* 2025;**23**:158.
59. Haminiuk CWI, Maciel GM, Plata-Oviedo MSV, Peralta RM. Phenolic compounds in fruits—an overview. *Int J Food Sci Technol* 2012;**47**:2023−44.
60. Zulkhairi Amin FA, Shafiq Cheng MZ, Sabri S, Ismail N, Chan KW, Mohd Esa N, et al. *In vivo* toxicity assessment of the probiotic *Bacillus amyloliquefaciens* HTI-19 isolated from stingless bee (*Heterotrigona itama*) honey. *Nutrients* 2023;**15**:2390.
61. Zhai FG, Liang QC, Wu YY, Liu JQ, Liu JW. Red ginseng polysaccharide exhibits anticancer activity through GPX4 downregulation-induced ferroptosis. *Pharm Biol* 2022;**60**:909−14.
62. An BK, Cho BL, You SJ, Paik HD, Chang HI, Kim SW, et al. Growth performance and antibody response of broiler chicks fed yeast derived β-glucan and single-strain probiotics. *Asian Austral J Anim Sci* 2008; **21**:1027−32.
63. Chen L, Ma Y, Ma X, Liu L, Jv X, Li A, et al. TFEB regulates cellular labile iron and prevents ferroptosis in a TfR1-dependent manner. *Free Radic Biol Med* 2023;**208**:445−57.
64. Nair A, Jacob S. A simple practice guide for dose conversion between animals and human. *J Basic Clin Pharm* 2016;**7**:27.
65. Zimmer C, Dorea C. Enumeration of *Escherichia coli* in probiotic products. *Microorganisms* 2019;**7**:437.
66. Sana MK, Abdullah SM, Ehsan H, Abdullah S, Ehsan A, Sharif MA, et al. Comparing the efficacy of cyclophosphamide *versus* lenalidomide in combination with bortezomib for newly diagnosed multiple myeloma treatment: a systematic review. *Blood* 2020;**136**:42.
67. Lu J, Huang D, Liu R, Zhu H, Wang D, Zhao Y, et al. Extracellular matrix-inspired dendrimer nanogels encapsulating cyclophosphamide for systemic sclerosis treatment. *ACS Nano* 2025;**19**:4672−83.
68. Wu F, Huang H. Surface morphology and protective effect of *Hericium erinaceus* polysaccharide on cyclophosphamide-induced immunosuppression in mice. *Carbohydr Polym* 2021;**251**:116930.
69. Zhao H, Li Y, Shi H, Niu M, Li D, Zhang Z, et al. Prodrug nanoparticles potentiate tumor chemo-immunometabolic therapy by disturbing oxidative stress. *J Control Release* 2022;**352**:909−19.
70. Asantewaa G, Tuttle ET, Ward NP, Kang YP, Kim Y, Kavanagh ME, et al. Glutathione synthesis in the mouse liver supports lipid abundance through NRF2 repression. *Nat Commun* 2024;**15**:6152.

71. Fu YJ, Zhao X, Wang LY, Li K, Jiang N, Zhang ST, et al. A gas therapy strategy for intestinal flora regulation and colitis treatment by nanogel-based multistage no delivery microcapsules. *Adv Mater* 2024; **36**:2309972.
72. Zhu G, Jiang Y, Yao Y, Wu N, Luo J, Hu M, et al. Ovotransferrin ameliorates the dysbiosis of immunomodulatory function and intestinal microbiota induced by cyclophosphamide. *Food Funct* 2019;**10**: 1109−22.
73. Gibiino G, Lopetuso LR, Scaldaferri F, Rizzatti G, Binda C, Gasbarrini A. Exploring bacteroidetes: metabolic key points and immunological tricks of our gut commensals. *Dig Liver Dis* 2018;**50**: 635−9.
74. Yu B, Zhang D, Wu Y, Tao W, Luorong Q, Luo J, et al. A new polysaccharide from Hawk tea: structural characterization and immunomodulatory activity associated with regulating gut microbiota. *Food Chem* 2023;**418**:135917.
75. Zhao Y, Yan Y, Zhou W, Chen D, Huang K, Yu S, et al. Effects of polysaccharides from bee collected pollen of chinese wolfberry on immune response and gut microbiota composition in cyclophosphamide-treated mice. *J Funct Foods* 2020;**72**:104057.
76. Longhi MS. *Lactobacillus reuteri* joins the liver autoimmune arena. *Cell Host Microbe* 2022;**30**:901−3.
77. Decout A, Krasias I, Roberts L, Gimeno Molina B, Charenton C, Brown Romero D, et al. *Lactobacillus crispatus* S-layer proteins modulate innate immune response and inflammation in the lower female reproductive tract. *Nat Commun* 2024;**15**:10879.
78. He X, McLean JS, Edlund A, Yooseph S, Hall AP, Liu SY, et al. Cultivation of a human-associated TM7 phylotype reveals a reduced genome and epibiotic parasitic lifestyle. *Proc Natl Acad Sci U S A* 2015;**112**:244−9.
79. Yao Y, Cai X, Fei W, Ye Y, Zhao M, Zheng C. The role of short-chain fatty acids in immunity, inflammation and metabolism. *Crit Rev Food Sci* 2020;**62**:1−12.
80. Wu W, Sun M, Chen F, Cao AT, Liu H, Zhao Y, et al. Microbiota metabolite short-chain fatty acid acetate promotes intestinal IgA response to microbiota which is mediated by GPR43. *Mucosal Immunol* 2017;**10**:946−56.
81. Kleuskens MTA, Haasnoot ML, Herpers BM, Ampting MTJv, Bredenoord AJ, Garssen J, et al. Butyrate and propionate restore interleukin 13-compromised esophageal epithelial barrier function. *Allergy* 2021;**77**:1510−21.
82. Nobs SP, Natali S, Pohlmeier L, Okreglicka K, Schneider C, Kurrer M, et al. PPARγ in dendritic cells and T cells drives pathogenic type-2 effector responses in lung inflammation. *J Exp Med* 2017;**214**:3015−35.
83. Van Ginderachter JA, Meerschaut S, Liu Y, Brys L, De Groeve K, Hassanzadeh Ghassabeh G, et al. Peroxisome proliferator-activated receptor (PPAR) ligands reverse CTL suppression by alternatively activated (M2) macrophages in cancer. *Blood* 2006;**108**:525−35.
84. Zhang Y, Liu Y, Zhang M, Li G, Zhu S, Xie K, et al. Clinical relevance and drug modulation of PPAR signaling pathway in triple-negative breast cancer: a comprehensive analysis. *PPAR Res* 2024;**2024**: 4164906.
85. Prat M, Coulson K, Blot C, Jacquemin G, Romano M, Renoud ML, et al. PPARγ activation modulates the balance of peritoneal macrophage populations to suppress ovarian tumor growth and tumor-induced immunosuppression. *J Immunother* 2023;**11**:e007031.
86. Byndloss Mariana X, Olsan Erin E, Rivera-Chávez Fabian, Tiffany Connor R, Cevallos Stephanie A, Lokken Kristen L, et al. Microbiota-activated PPAR-γ signaling inhibits dysbiotic *Enterobacteriaceae* expansion. *Science* 2017;**357**:570−5.
87. Chen B, Guan L, Wu C, Gong Y, Wu L, Zhang M, et al. Gut microbiota−butyrate−PPARγ axis modulates adipose regulatory T cell population. *Adv Sci* 2025;**12**:2411086.
88. Li LF, Yue GGL, Chan BCL, Zeng Q, Han QB, Leung PC, et al. *Rubinoboletus ballouii* polysaccharides exhibited immunostimulatory activities through Toll-like receptor-4 *via* NF-κB pathway. *Phytother Res* 2020;**35**:2108−18.
89. Yamashita M, Passegué E. TNF-α coordinates hematopoietic stem cell survival and myeloid regeneration. *Cell Stem Cell* 2019;**25**: 357−372.e7.
90. Garavelli S, Bruzzaniti S, Tagliabue E, Prattichizzo F, Di Silvestre D, Perna F, et al. Blood co-circulating extracellular micrornas and immune cell subsets associate with type 1 diabetes severity. *Int J Mol Sci* 2020;**21**:477.
91. Xiao H, Guo Y, Li B, Li X, Wang Y, Han S, et al. M2-like tumor-associated macrophage-targeted codelivery of STAT6 inhibitor and IKKβ siRNA induces M2-to-M1 repolarization for cancer immunotherapy with low immune side effects. *ACS Cent Sci* 2020;**6**: 1208−22.
92. Zheng B, Wang D, Qiu X, Luo G, Wu T, Yang S, et al. Trajectory and functional analysis of PD-1^{high} $CD4^{+}CD8^{+}$ T cells in hepatocellular carcinoma by single-cell cytometry and transcriptome sequencing. *Adv Sci* 2020;**7**:2000224.
93. Sisi Lin SM, Juanjuan Li, Hou Weiliang, Pan Chao, Liu Jinyao. Mucosal immunity-mediated modulation of the gut microbiome by oral delivery of probiotics into peyer's patches. *Sci Adv* 2021;**7**: eabf0677.
94. Meza-Perez S, Liu M, Silva-Sanchez A, Morrow CD, Eipers PG, Lefkowitz EJ, et al. *Proteobacteria* impair anti-tumor immunity in the omentum by consuming arginine. *Cell Host Microbe* 2024;**32**: 1177−1191.e7.
95. Shahid S, Abid R, Ajmal W, Almuqbil M, Almadani ME, Khan Y, et al. Antibiotic resistance genes prediction *via* whole genome sequence analysis of stenotrophomonas maltophilia. *J Infect Public Health* 2024;**17**:236−44.
96. Wang N, Sun T, Xu J. Tumor-related microbiome in the breast microenvironment and breast cancer. *J Cancer* 2021;**12**:4841−8.
97. Zhang J, Xie Q, Huo X, Liu Z, Da M, Yuan M, et al. Impact of intestinal dysbiosis on breast cancer metastasis and progression. *Front Oncol* 2022;**12**:1037831.